Proceedings

of the

GMP-X Conference on Geometry and Applied Mathematics

April 10–11, 2026
Marrakesh, Morocco

Preface

The GMP outreach conference series bridges the gap between the international and local research communities in countries that are often underrepresented internationally by eXtending the GMP conference series and offering an eXtraordinary eXperience in eXciting places. GMP-X 2026 was the first conference in this new series. It took place at Cadi Ayyad University in Marrakesh, Morocco on April 10–11, 2026 and celebrated the 64th birthday of Prof. Aziz Ikemakhen.

Bringing together leading experts, emerging scholars, and students, the event fostered collaboration and the exchange of knowledge and provided a dynamic platform for sharing innovative ideas, methodologies, and applications in geometric modeling and processing, as well as in applied mathematics more broadly.

The GMP-X conference inspired local researchers to engage actively in this vibrant area of research and to encourage their contributions to its ongoing development. It also offered PhD students and early-career researchers the opportunity to discover the latest advances in geometric modeling and its diverse applications.

The conference topics aligned with the themes of the GMP conference series, focusing on established research topics in geometric modeling and processing. Contributions came from the following areas:

- Geometry (theoretical and applied)
- Numerical and Applied Mathematics
- Computational Engineering
- Computer Graphics
- Computational Geometry
- Geometry Processing
- Computer Vision
- Geometric Deep Learning
- Related disciplines intersecting with geometric methods
- Applications of geometric approaches

This broader inclusion was intended to foster interdisciplinary collaboration and to highlight the relevance of geometric approaches across various domains.

Scientific Committee

- *Noureddine Alaa*, Cadi Ayyad University, Morocco
- *Falai Chen*, University of Science and Technology of China, China
- *Francesco Dell'Accio*, Università della Calabria, Italy
- *Kai Hormann*, Università della Svizzera italiana, Switzerland
- *Aziz Ikemakhen*, Cadi Ayyad University, Morocco
- *Jörg Peters*, University of Florida, USA
- *Hartmut Prautzsch*, Karlsruhe Institute of Technology, Germany

Organizers

- *Kai Hormann*, Università della Svizzera italiana, Switzerland
- *Aziz Ikemakhen*, Cadi Ayyad University, Morocco
- *Mahrou Khalid*, Cadi Ayyad University, Morocco

Sponsors

- Cadi Ayyad University, Morocco
- Università della Svizzera italiana, Switzerland

Table of Contents

Preface i

Table of Contents iii

Conference Program v

Keynote Talks 1

Quad meshes in sphere geometries 3
Helmut Pottmann

Frequency domain Bernstein-Bézier finite element solver for modelling elastic and electromagnetic short waves 4
Abdellah El kacimi

Vibrations of geometric shapes 5
Konrad Polthier

On the Hermitian structures of the sequence of tangent bundles of an affine manifold endowed with a Riemannian metric 6
Mohammed Boucetta

Contributed Talks 7

Aligning geometry and language in free-form architectural design 9
Andrea Favilli

Cage-based dynamic mesh compression 10
Navdeep Singh Bedi

Deep learning approaches for inverse problems in parabolic partial differential equations 11
Fadwa Zaidane

A physics-informed neural network approach for simulating a class of T-periodic cooperative parabolic systems 12
Oumaima Bonouali

Physics-informed neural networks for solving inverse problem in electro-cardiography 13
Salma Bakadir

Neuron-wise variational spline activations via intrinsic elastic energy minimization 14
Soumia Ngadi

Asymptotic solver for Mathieu equation with high excitation frequency 15
Mustapha Kzaz

Cubic serendipity coordinates over arbitrary polygonal elements 16
Marta Celio

Isogeometric approximation of Laplace eigenvalue problems on the disk using UTA-splines 17
Manal Naimi

RF-based construction of a non-uniform subdivision scheme from a uniform scheme 18
Amine Arhandou

Spline Orbifold Spaces 19
Hartmut Prautzsch

Volumetric decomposition for optimized rigid mold disassembly 20
Luca Garau

Dimensionality reduction and first-order Riemannian optimization: Applications in face recognition 21
Hajar Lafdili

Adaptive edge detection using symmetric q-derivatives: generalization of the Sobel, Prewitt, Roberts, and Canny operators 22
Ranya Salouani

On the concept of symmetry 23
Abderrazzak Benroummane

Symplectic Leibniz algebras 24
Fatima-Ezzahrae Abid

Flat left-invariant Lorentzian metrics on almost abelian Lie groups 25
Hicham Lebzioui

Natural Ricci solitons on tangent and unit tangent bundles 26
Noura Amri

The volume of a vector field on a Riemannian manifold 27
Oumaima Bradaai

Short Papers 29

Positive hyperbolic barycentric coordinates for non-convex polygons 31
Alaa Eddine Bensad

A learning-assisted algorithmic framework for constructing a generalized Voronoi graph representation in grid space 39
Joms Antony

Projection-based structural element extraction from point clouds 45
Diana Marin

Posters 51

Image vectorization with generalized Coons patches 53
Yan Jing

Speaker Index 55

Conference Program — Day 1

	Friday, April 10
08:30–09:00	**Registration**
09:00–09:20	**Opening**
	Session 1 — *Hartmut Prautzsch* (Chair)
	Keynote Talk
09:20–10:20	*Helmut Pottmann* — Quad meshes in sphere geometries
	Geometry Processing
10:20–10:40	*Andrea Favilli* — Aligning geometry and language in free-form architectural design
10:40–11:00	*Alaa Eddine Bensad* — Positive hyperbolic barycentric coordinates for non-convex polygons *(short paper)*
11:00–11:20	*Navdeep Singh Bedi* — Cage-based dynamic mesh compression
11:20–11:50	**Coffee Break**
	Session 2 — *Konrad Polthier* (Chair)
	Geometric Deep Learning
11:50–12:10	*Fadwa Zaidane* — Deep learning approaches for inverse problems in parabolic partial differential equations
12:10–12:30	*Oumaima Bonouali* — A physics-informed neural network approach for simulating a class of T-periodic cooperative parabolic systems
12:30–12:50	*Salma Bakadir* — Physics-informed neural networks for solving inverse problem in electro-cardiography
12:50–13:10	*Soumia Ngadi* — Neuron-wise variational spline activations via intrinsic elastic energy minimization
13:10–15:30	**Prayer & Lunch Break**
	Session 3 — *Mohammed Boucetta* (Chair)
	Keynote Talk
15:30–16:30	*Abdellah El kacimi* — Frequency domain Bernstein-Bézier finite element solver for modelling elastic and electromagnetic short waves
	Numerical Methods
16:30–16:50	*Mustapha Kzaz* — Asymptotic solver for Mathieu equation with high excitation frequency
16:50–17:10	*Marta Celio* — Cubic serendipity coordinates over arbitrary polygonal elements
17:10–17:30	*Manal Naimi* — Isogeometric approximation of Laplace eigenvalue problems on the disk using UTA-splines
20:00–23:00	**Social Dinner**

Conference Program — Day 2

	Saturday, April 11
	Session 4 — *Kai Hormann* (Chair)
	Keynote Talk
09:00–10:00	*Konrad Polthier* — Vibrations of geometric shapes
	Curves, Surfaces, and Volumes
10:00–10:20	*Amine Arhandou* — RF-based construction of a non-uniform subdivision scheme from a uniform scheme
10:20–10:40	*Hartmut Prautzsch* — Spline orbifold spaces
10:40–11:00	*Luca Garau* — Volumetric decomposition for optimized rigid mold disassembly
11:00–11:40	**Coffee Break & Poster Session**
	Session 5 — *Helmut Pottmann* (Chair)
	Geometric and Visual Computing
11:40–12:00	*Joms Antony* — A learning-assisted algorithmic framework for constructing a generalized Voronoi graph representation in grid space *(short paper)*
12:00–12:20	*Hajar Lafdili* — Dimensionality reduction and first-order Riemannian optimization: Applications in face recognition
12:20–12:40	*Ranya Salouani* — Adaptive edge detection using symmetric q-derivatives: generalization of the Sobel, Prewitt, Roberts, and Canny operators
12:40–13:00	*Diana Marin* — Projection-based structural element extraction from point clouds *(short paper)*
13:00–14:30	**Lunch Break**
	Session 6 — *Aziz Ikemakhen* (Chair)
	Keynote Talk
14:30–15:30	*Mohammed Boucetta* — On the Hermitian structures of the sequence of tangent bundles of an affine manifold endowed with a Riemannian metric
	Geometric Structures
15:30–15:50	*Abderrazzak Benroummane* — On the concept of symmetry
15:50–16:10	*Fatima-Ezzahrae Abid* — Symplectic Leibniz algebras
16:10–16:30	*Hicham Lebzioui* — Flat left-invariant Lorentzian metrics on almost abelian Lie groups
16:30–17:00	**Coffee Break**
	Session 7 — *Mustapha Kzaz* (Chair)
	Differential Geometry
17:00–17:20	*Noura Amri* — Natural Ricci solitons on tangent and unit tangent bundles
17:20–17:40	*Oumaima Bradaai* — The volume of a vector field on a Riemannian manifold
17:40–18:00	**Closing**

Keynote Talks

— Keynote Talk —

Quad meshes in sphere geometries

Helmut Pottmann[1]

Abstract

Quad meshes play a key role in discrete differential geometry and various applications, including geometry processing, computational design and architecture. Some quad meshes can be seen as objects of classical sphere geometries. For example, the main discrete principal curvature parameterizations, namely circular meshes and conical meshes, are objects of the sphere geometries of Möbius and Laguerre, respectively. One can turn them into a Lie geometric structure, resulting in a smooth surface composed of Dupin cyclide patches. Moreover, the study of principal-symmetric meshes and their applications is naturally performed within sphere geometries. Finally, we consider sphere meshes all whose elements are defined within sphere geometry. Möbius geometric sphere meshes have spherical faces and circular edges. The Laguerre geometric counterparts are composed of planar, spherical and conical patches and the resulting surfaces are smooth for positive curvature. We address various approximation problems with such meshes and thereby encounter a new theoretical tool, namely generalized conjugate nets. The presentation illustrates the interplay of theory and applications and the alternation between smooth nets and their discrete counterparts.

Biography

Helmut Pottmann is a professor emeritus of applied geometry at TU Wien. He has had faculty positions in the US, in Germany and at King Abdullah University of Science and Technology in Saudi Arabia, where he has been founding director of the Visual Computing Center. His research interests are in applied geometry, classical geometry and discrete differential geometry with a focus on applications in architecture, computational design and fabrication. His work in architectural geometry has also found its way into real projects such as the Eiffel Tower Pavilions and the Museum of Islamic Art in the Louvre in Paris, or the Yas Island Marina Hotel in Abu Dhabi. He is a Fellow of SIAM and received the Eurographics Outstanding Technical Contributions Award and the Bezier Award of the Solid Modeling Association.

[1]TU Wien, Austria

— Keynote Talk —

Frequency domain Bernstein-Bézier finite element solver for modelling elastic and electromagnetic short waves

Abdellah El kacimi [1]

Abstract

This talk presents a high-order Bernstein-Bézier finite element (FE) discretisation for the efficient solution of time harmonic elastic and electromagnetic wave problems on unstructured triangular mesh grids. Yet high-order FEs have several benefits over standard FEs, the computational cost to set up the element matrices is a major issue in high-order computations. A key ingredient to address this drawback is to use low complexity procedures in building the local high order FE matrices, by exploiting the tensorial property of Bernstein polynomials and applying the sum factorisation method. To reduce the memory requirements, static condensation of the interior degrees of freedom is performed element-wise. The performance of the Bernstein–Bézier FEs is assessed on various benchmark tests, within a wide range of frequencies. The obtained results demonstrate the effectiveness of the proposed solver in coping with the pollution error, and its accuracy in resolving high order evanescent wave modes.

Biography

Dr. Abdellah El Kacimi is Professor of Applied Mathematics at Cadi University. Previously, he was involved as research-associate at Heriot-Watt University. His main research interests lie in computational modelling, with applications in fluid dynamic, wave problems and high speed railway. He has participated in numerous research projects funded by the European Commission and national agencies.

[1] Cadi Ayyad University, Morocco

— Keynote Talk —

Vibrations of geometric shapes

Konrad Polthier[1]

Abstract

Vibrations of musical strings are well understood by Fourier analysis while the vibrations of geometric shapes exhibit surprising properties triggered by careful choices of differential geometric energies. We will review solved problems and introduce novel approaches with applications in biology, computer graphics and crystallography, and in topology.

Biography

Konrad Polthier is full professor of mathematics at Freie Universität Berlin since 2005. He received his PhD from University of Bonn in 1994, and headed research groups at Technische Universität Berlin and Zuse Institute Berlin. His research focuses on discrete differential geometry, applied geometry, geometry processing, and mathematical visualization. Results from him have been applied in industry such as computer graphics, computer aided design, and architecture. Dr. Polthier has written and co-edited books on mathematical visualization and co-produced mathematical video films. His video *MESH – A Journey Through Discrete Geometry* (www.mesh-film.de), joint with Beau Janzen, has received several international awards. Polthier has served as conference chair on international conferences, including the International Geometry Summit, SGP, and SIAM Geometric Design. He serves as co-editor in chief of Computer Aided Geometric Design, and he supports mathematical outreach as chair of the Berlin Mathematical Society.

[1]Freie Universität Berlin, Germany

GMP-X Conference on Geometry and Applied Mathematics
April 10–11, 2026 · Marrakesh, Morocco

— Keynote Talk —

On the Hermitian structures of the sequence of tangent bundles of an affine manifold endowed with a Riemannian metric

Mohammed Boucetta[1]

Abstract

Let $(M, \nabla, \langle\ ,\ \rangle)$ be a manifold endowed with a flat torsionless connection ∇ and a Riemannian metric $\langle\ ,\ \rangle$ and $(T^kM)_{k\geq 1}$ the sequence of tangent bundles given by $T^kM = T(T^{k-1}M)$ and $T^1M = TM$. We show that, for any $k \geq 1$, T^kM carries a Hermitian structure (J_k, g_k) and a flat torsionless connection ∇^k and when M is a Lie group and $(\nabla, \langle\ ,\ \rangle)$ are left invariant, there is a Lie group structure on each T^kM, such that (J_k, g_k, ∇^k) are left invariant. It is well-known that (TM, J_1, g_1) is Kähler, if and only if $\langle\ ,\ \rangle$ is Hessian, i.e., in each system of affine coordinates $(x_1, \ldots, x_n)$, $\langle \partial_{x_i}, \partial_{x_j} \rangle = \frac{\partial^2 \phi}{\partial_{x_i} \partial_{x_j}}$. Having in mind many generalizations of the Kähler condition introduced re- cently, we give the conditions on $(\nabla, \langle\ ,\ \rangle)$ so that (TM, J_1, g_1) is balanced, locally conformally balanced, locally conformally Kähler, pluriclosed, Gauduchon, Vaismann, or Calabi-Yau with torsion. Moreover, we can control at the level of $(\nabla, \langle\ ,\ \rangle)$ the conditions insuring that some (T^kM, J_k, g_k) or all of them satisfy a generalized Kähler condition. For instance, we show that there are some classes of $(M, \nabla, \langle\ ,\ \rangle)$ such that, for any $k \geq 1$, (T^kM, J_k, g_k) is balanced non-Kähler and Calabi-Yau with torsion. By carefully studying the geometry of $(M, \nabla, \langle\ ,\ \rangle)$, we develop a powerful machinery to build a large classes of generalized Kähler manifolds.

Biography

Mohamed Boucetta is a Professor at Cadi-Ayyad University. His research interest are differential geometry and non associative algebras.

[1]Cadi-Ayyad University, Morocco

Contributed Talks

GMP-X Conference on Geometry and Applied Mathematics
April 10–11, 2026 · Marrakesh, Morocco

Aligning geometry and language in free-form architectural design

Andrea Favilli[1,2] · Francesco Laccone[1] · Paolo Cignoni[1] · Luigi Malomo[1] · Daniela Giorgi[1]

Abstract

Architectural Geometry [3] develops geometric strategies to address complex design and fabrication challenges of free-form shapes. Recently, Artificial Intelligence has entered this domain, integrating neural networks into shape optimization pipelines [1, 2]. Contributing to this evolving field, this talk proposes a framework that learns a shared latent space between free-form geometries and their textual descriptions, enabling designers to explore shape space through natural language. By leveraging semantic similarity defined by metric proximity in a joint embedding space, the approach aligns language with the corresponding architectural form.

The framework unfolds in two phases: domain-specific dataset generation with paired textual descriptions, and joint latent representation learning. Geometry processing is central both to generating free-form NURBS surfaces resembling those created by human designers and to extracting design-oriented descriptors, which are converted into captions through scripted prompting of large language models. A 3D autoencoder learns compact embeddings that capture global shape characteristics, and a contrastive alignment maps shape and text representations into a shared latent space, enabling cross-modal retrieval and semantic exploration.

Our work leverages shape analysis for encoding designers' desiderata such as smoothness, structural expressiveness, and spatial continuity into dedicated features, framing AI as a geometry-aware assistant for early-stage architectural design.

References

[1] A. Favilli, F. Laccone, P. Cignoni, L. Malomo, and D. Giorgi. Geometric deep learning for statics-aware grid shells. *Computers & Structures*, 292:107238, Feb. 2024.

[2] A. Favilli, F. Laccone, P. Cignoni, L. Malomo, and D. Giorgi. Optimizing Free-Form Grid Shells with Reclaimed Elements under Inventory Constraints. *Computer Graphics Forum*, 44(2):e70047, 2025.

[3] H. Pottmann, M. Eigensatz, A. Vaxman, and J. Wallner. Architectural geometry. *Computers & Graphics*, 47:145–164, Apr. 2015.

[1]ISTI - CNR, Italy
[2]Department of Computer Science, University of Pisa, Italy

GMP-X Conference on Geometry and Applied Mathematics
April 10–11, 2026 · Marrakesh, Morocco

Cage-based dynamic mesh compression

Navdeep Singh Bedi[1] · Zuzana Káčereková[2] · Filip Hácha[2] · Libor Váša[2] · Kai Hormann[1]

Abstract

Cage-based deformation is a convenient way to create 3D animations of high-resolution meshes by means of moving the vertices of a low-resolution control mesh. The resulting animation is a dynamic mesh, that is, a sequence of meshes with shared connectivity, which is controlled entirely by the corresponding dynamic cage. In this paper, we propose to invert this process and approximate a given dynamic mesh sequence with a cage-based animation of the average mesh of that sequence. We can then represent the dynamic mesh in a very compact way by compressing the dynamic cage sequence and the average mesh. We use mean value coordinates [1] for binding the mesh to the cage and publicly available state-of-the-art algorithms for computing the average mesh [5] and compressing static [2, 3] and dynamic meshes [4, 3]. Apart from the general idea of inverse cage-based animation, we describe a novel approach for automatically creating a motion-aware cage for the average mesh as well as a method for optimizing the latter. Compared to the compression of the given dynamic mesh, our overall pipeline turns out to give better results, in particular at high compression rates.

References

[1] M. S. Floater, G. Kós, and M. Reimers. Mean value coordinates in 3D. *Computer Aided Geometric Design*, 22(7):623–631, Oct. 2005.

[2] O. Sorkine, D. Cohen-Or, and S. Toledo. High-pass quantization for mesh encoding. In *Proceedings of the First Symposium on Geometry Processing*, SGP '03, pages 42–51, Aire-la-Ville, June 2003. Eurographics Association.

[3] L. Váša and J. Dvořák. Error propagation control in Laplacian mesh compression. *Computer Graphics Forum*, 37(5):61–70, Aug. 2018.

[4] L. Váša, S. Marras, K. Hormann, and G. Brunnett. Compressing dynamic meshes with geometric Laplacians. *Computer Graphics Forum*, 33(2):145–154, May 2014.

[5] T. Winkler, J. Drieseberg, M. Alexa, and K. Hormann. Multi-scale geometry interpolation. *Computer Graphics Forum*, 29(2):309–318, May 2010.

[1]Università della Svizzera italiana, Lugano, Ticino, Switzerland
[2]University of West Bohemia, Plzeň, Czechia

GMP-X Conference on Geometry and Applied Mathematics
April 10–11, 2026 · Marrakesh, Morocco

Deep Learning Approaches for Inverse Problems in Parabolic Partial Differential Equations

Fadwa Zaidane[1] · Khalid Atifi[1] · El-Hassan Essoufi[1] · Abdeslam Talha[1]

Abstract

Inverse problems for parabolic partial differential equations play a central role in many scientific and engineering applications and can be challenging due to ill-posedness and instability. In this work, we inquire into data-driven approaches for the recovery of unknown parameters in nonlinear parabolic PDEs using deep learning approaches. We explore the use of physics-informed learning strategies and neural operators architectures to estimate hidden quantities from final observations. We also discuss fundamental theoretical issues related to well posdness of inverse formulations, addressing classical Hadamard criteria. Preliminary results are shown to evaluate the behavior of the proposed methodology and to analyze the influence of the model design on reconstruction performance. This work is ongoing and aims to contribute toward providing efficient and flexible tools for solving inverse problems using machine learning tools.

References

[1] Maziar Raissi, Paris Perdikaris, and George Em Karniadakis. Physics-informed neural networks: A deep learning framework for solving forward and inverse problems involving nonlinear partial differential equations. *Journal of Computational Physics*, 378:686–707, 2019.

[2] Zongyi Li, Nikola Kovachki, Kamyar Azizzadenesheli, Burigede Liu, Kaushik Bhattacharya, Andrew Stuart, and Animashree Anandkumar. Fourier neural operator for parametric partial differential equations. *arXiv preprint arXiv:2010.08895*, 2020.

[3] Yu.Ya. Belov. *Inverse Problems for Partial Differential Equations*. Inverse and Ill-Posed Problems Series. IIIVSPIII, Utrecht-Boston-Koln-Tokyo, 2002.

[4] Soufiane Abid, Khalid Atifi, El-Hassan Essoufi, and Abderrahim Zafrar. Identification of source term in a nonlinear degenerate parabolic equation with memory. *Applications of Mathematics*, 2024. Received February 25, 2023; Published online February 7, 2024.

[1, 2, 3, 4].

[1]Laboratory of Mathematics, Computer Science and Engineering Sciences (MISI) - Hassan 1 University Settat 26000, Morocco

GMP-X Conference on Geometry and Applied Mathematics
April 10–11, 2026 · Marrakesh, Morocco

A Physics-Informed Neural Network Approach for Simulating a Class of T-Periodic Cooperative Parabolic Systems

Oumaima Bonouali[1] · Fatima Aqel[2] · Hamza Alaa[3]

Abstract

This work is devoted to the analysis of weak T-periodic solutions for a class of nonlinear cooperative parabolic systems subject to Neumann boundary conditions. Using the framework of ordered Banach spaces, we establish an existence criterion based on a monotone iterative scheme and the method of sub- and supersolutions. Under Carathéodory-type assumptions and a structural cooperativity condition, the existence of extremal periodic solutions is obtained, while uniqueness and stability follow from a small Lipschitz condition on the nonlinearities.

The theoretical results are applied to a periodic reaction–diffusion model describing the spatiotemporal evolution of neurodegenerative diseases. To complement the analytical study, a Physics-Informed Neural Network approach is proposed to numerically approximate the periodic regimes. The numerical experiments confirm the theoretical predictions and demonstrate the robustness and efficiency of the proposed method in biologically relevant scenarios.

Key words: Periodic, cooperative system,Physics-Informed Neural Networks (PINNs) .

References

[1] H. Alaa, F. Aqel, A. H. Bentbib, and N. E. Alaa, "Mathematical analysis of a class of cooperative differential periodic system," *Open J. Math. Sci.*, submitted for publication, 2026.

[2] H. Amann, "Fixed point equations and nonlinear eigenvalue problems in ordered Banach spaces," *SIAM Review*, vol. 18, no. 4, pp. 620–709, 1976.

[3] C. Cosner and A. C. Lazer, "Stable coexistence states in the Volterra-Lotka competition model with diffusion," *SIAM Journal on Applied Mathematics*, vol. 44, no. 6, pp. 1112–1132, 1984.

[4] D. Daners and P. Koch Medina, *Abstract Evolution Equations, Periodic Problems and Applications*. Longman Scientific & Technical, 1992.

[5] M. J. Esteban, "On periodic solutions of superlinear parabolic problems," *Transactions of the American Mathematical Society*, vol. 293, no. 1, pp. 171–189, 1986.

[6] L. C. Evans, *Partial Differential Equations*, 2nd ed. American Mathematical Society, 2010.

[7] P. Hess, *Periodic-Parabolic Boundary Value Problems and Positivity*. Longman Scientific & Technical, 1991.

[8] O. A. Ladyzhenskaya, V. A. Solonnikov, and N. N. Ural'tseva, *Linear and Quasi-linear Equations of Parabolic Type*. American Mathematical Society, 1968.

[9] J.-L. Lions and E. Magenes, *Non-Homogeneous Boundary Value Problems and Applications*, Vol. 1. Springer-Verlag, Berlin-Heidelberg-New York, 1972. Translated from French by P. Kenneth.

[10] D. H. Sattinger, "Monotone methods in nonlinear elliptic and parabolic boundary value problems," *Indiana University Mathematics Journal*, vol. 21, no. 11, pp. 979–1000, 1972.

[11] J. Simon, "Compact sets in the space $L^p(0,T;B)$," *Annali di Matematica Pura ed Applicata*, vol. 146, pp. 65

[1]LAVETE Laboratory, Faculty of Sciences and Technics, Hassan First University, Settat 577 Casablanca Road, Morocco
[2]LAVETE Laboratory, Faculty of Sciences and Technics, Hassan First University, Settat 577 Casablanca Road, Morocco
[3]Laboratory LAMAI, Faculty of Science and Technology, Cadi Ayyad University, 40000 Marrakesh, Morroco

GMP-X Conference on Geometry and Applied Mathematics
April 10–11, 2026 · Marrakesh, Morocco

Physics-Informed Neural Networks for solving inverse problem in electro-cardiography

Salma Bakadir [1] · Mostafa Bendahmane [2] · Noureddine Alaa [1]

Abstract

We study the inverse problem in electrocardiography, which aims to reconstruct the cardiac surface potential from measurements recorded on the torso. The forward model is based on a Laplace-type equation that represents the torso as a passive conductor [1]. Since the inversion is ill-posed, we cast it as a regularized optimization problem and compute the gradient through an adjoint formulation [2]. The reconstruction is performed using Physics-Informed Neural Networks (PINNs), which enforce the governing physical constraints during training [4]. Numerical results show a stable recovery on simplified geometries, consistent with standard approaches in inverse ECG [3].

References

[1] R. C. Barr, M. I. Ramsey, and M. S. Spach. Relating epicardial to body surface potential distributions by means of transfer coefficients based on geometry measurements. *IEEE Transactions on Biomedical Engineering*, 1977.

[2] A. Charkaoui, A. El Badia, and N. E. Alaa. An efficient and robust algorithm for source reconstruction in the helmholtz equation. *Inverse Problems in Science and Engineering*, 29(13):2944–2970, 2021.

[3] A. Lopez Rincon, M. Bendahmane, and B. Ainseba. Two-step genetic algorithm to solve the inverse problem in electrocardiography for cardiac sources. *Computer Methods in Biomechanics and Biomedical Engineering: Imaging and Visualization*, 2(3):129–137, 2014.

[4] M. Raissi, P. Perdikaris, and G. E. Karniadakis. Physics-informed neural networks: A deep learning framework for solving forward and inverse problems involving nonlinear partial differential equations. *Journal of Computational Physics*, 2019.

[1]Department of Mathematics, Faculty of Sciences and Technology of Marrakech, Cadi Ayyad University
[2]Mathematical institute of Bordeaux and INRIA-Sud-Ouest, Bordeaux university, France

GMP-X Conference on Geometry and Applied Mathematics
April 10–11, 2026 · Marrakesh, Morocco

Neuron-wise Variational Spline Activations via Intrinsic Elastic Energy Minimization

Soumia NGADI[1] · Mohamed LAMII[1]

Abstract

We propose a variational framework for neural networks in which neuron activations are modeled as elastic functions that have their own energy. Each activation function is parameterized in a spline basis and regularized through a quadratic elastic energy defined directly at the coefficient level, without directly usig derivatives. The preactivation signal acts as an external excitation, while the elastic energy enforces internal regularity independently of the data. This formulation yields a clear physical interpretation of neurons as elastic systems that adjust to balance external forces against their internal rigidity. The proposed approach unifies spline theory, variational mechanics, and neural network regularization, providing stability, interpretability, and mathematical structure.

[1]LANO Laboratory, Department of Mathematics, Faculty of Sciences, Mohammed First University, Oujda, Morocco.

GMP-X Conference on Geometry and Applied Mathematics
April 10–11, 2026 · Marrakesh, Morocco

Asymptotic solver for Mathieu equation with high excitation frequency

Mustapha Kzaz[1] · Fatima Maach[1]

Abstract

The Mathieu equation

$$x''(t)+\gamma x'(t)+(a-\sum_{|k|=1}^{N} c_k e^{ik\omega t})x(t)=f(t),\ \omega\gg 1,$$

is a classical model of parametric resonance with numerous applications in physics and engineering. In the high-frequency regime, the multiple scales method provides a formal framework for analyzing such problems. However, it is typically applied only to low orders and does not yield a systematic recursive scheme or rigorous error bounds.

In this paper, we develop a constructive extension of the multiple-scale approach. Starting from a Fourier ansatz expansion, we derive an asymptotic solution in inverse powers of ω, whose coefficients are obtained recursively and incorporate both slowly varying and oscillatory components. We also provide a rigorous estimate of the error of the truncated expansion, showing that the remainder is uniformly $O(\omega^{-(R-1)})$.

Finally, we implement the recursive scheme and validate it through numerous numerical examples. The study investigates two mathematically distinct and physically relevant asymptotic regimes: Regime I: weak high-frequency modulation, typical of problems involving weak periodic modulation, such as vibrational control or wave propagation in weakly periodic environments (see [2, 6]). Regime II: strong high-frequency modulation, describing systems found, for instance, in plasma physics or in mechanical systems with large-amplitude vibration (see [1, 3, 4, 5]).

References

[1] L. Allen and J. H. Eberly, *Optical Resonance and Two-Level Atoms*, Dover Publications, New York, 1987.

[2] V. I. Arnold, *Mathematical Methods of Classical Mechanics*, Springer, New York, 1989.

[3] E. Hairer and C. Lubich, Long-time behaviour of oscillatory differential equations, *Acta Numerica*, **9** (2000), pp. 1–89.

[4] E. Hairer, C. Lubich, and G. Wanner, *Geometric Numerical Integration: Structure-Preserving Algorithms for Ordinary Differential Equations*, 2nd ed., Springer, Berlin, 2006.

[5] A. Iserles, *Highly Oscillatory Problems*, Cambridge University Press, Cambridge, 2020.

[6] A. H. Nayfeh and D. T. Mook, *Nonlinear Oscillations*, Wiley, New York, 1979.

[1]University Cadi-Ayyad, UCA, FST-Gueliz, Department of Mathematics, Marrakech, Morocco

GMP-X Conference on Geometry and Applied Mathematics
April 10–11, 2026 · Marrakesh, Morocco

Cubic serendipity coordinates over arbitrary polygonal elements

Marta Celio[1]

Abstract

This work provides a construction for 2D cubic serendipity coordinates based on the work by Hackemack and Ragusa [2]. The serendipity coordinates are obtained as linear combinations of products of generalized barycentric coordinates (GBCs), in particular mean value coordinates [1]. From these serendipity coordinates, an equal number of interpolation nodes and functions are defined, once again making use of linear combinations. The interpolation functions are then used for solving 2D FEM problems with polygonal elements. Inheriting the properties of mean value coodinates, these functions can be defined over convex, weakly convex and concave polygons with any number of vertices; moreover, they provide a quartic convergence order in the L^2 norm. On triangular elements, an additional interpolation node is added at the triangle's centroid.

References

[1] M. S. Floater. Mean value coordinates. *Computer Aided Geometric Design*, 20(1):19–27, 2003.

[2] M. W. Hackemack and J. C. Ragusa. Quadratic serendipity discontinuous finite element discretization for S_N transport on arbitrary polygonal grids. *Journal of Computational Physics*, 374:188–212, 2018.

[1]Faculty of Informatics, Università della Svizzera italiana, Lugano

GMP-X Conference on Geometry and Applied Mathematics
April 10–11, 2026 · Marrakesh, Morocco

Isogeometric Approximation of Laplace Eigenvalue Problems on the Disk Using UAT-Splines

Manal Naimi[1,2] · Mohamed Lamnii[1]

Abstract

We propose an isogeometric framework for the approximation of Laplace eigenvalue problems on the disk using UAT-splines. Unlike classical B-splines and NURBS-based approaches, the proposed construction incorporates trigonometric functions directly within the angular approximation space, allowing the exact representation of circular geometry without resorting to rational parametrizations. In particular, cosine and sine functions are reproduced exactly in the discrete space, eliminating the need for NURBS weights while preserving geometric exactness.

References

[1] Berger, A. (2015). Optimisation du spectre du Laplacien avec conditions de Dirichlet et Neumann dans R2 et R3. https://doi.org/10.35662/unine-thesis-2470

[2] Brézis, H. (1999). Analyse fonctionnelle : Théorie et applications.

[3] Cottrell, J. A., Hughes, T. J. R., and Bazilevs, Y. (2009). Isogeometric analysis. https://doi.org/10.1002/9780470749081

[4] Hughes, T., Cottrell, J., and Bazilevs, Y. (2005). Isogeometric analysis : CAD, finite elements, NURBS, exact geometry and mesh refinement. Computer Methods In Applied Mechanics And Engineering, 194(39-41), 4135-4195. https://doi.org/10.1016/j.cma.2004.10.008

[5] Schumaker, L. (2007). Spline Functions : Basic Theory. Dans Cambridge University Press eBooks. https://doi.org/10.1017/cbo9780511618994

[1]Laboratory LANO, Faculty of sciences, University Mohamed First, Oujda, Morocco
[2]Research center, School of Higher Engineering studies, EHEI, Oujda, Morocco

GMP-X Conference on Geometry and Applied Mathematics
April 10–11, 2026 · Marrakesh, Morocco

RF-Based Construction of a Non-Uniform Subdivision Scheme from a Uniform Scheme

Amine Arhandou [1*] · Mohamed-Yassir Nour [2] · Abdellah Lamnii [1]

Abstract

Subdivision schemes are widely used in geometric modeling to generate smooth curves and surfaces from a discrete set of points called a control polygon. In classical formulations, many subdivision schemes are defined as uniform schemes, in which the refinement parameters remain constant over the entire control polygon. However, the use of global parameters can limit the scheme's ability to adapt to local geometric variations.
In this work, we propose an artificial intelligence-based approach that transforms a uniform hyperbolic subdivision scheme into a non-uniform adaptive scheme. The main idea is to automatically predict local tension parameters from the geometric descriptors of the control polygon using a learning model. The predicted parameters are then integrated into the subdivision process while preserving the analytical structure of the initial hyperbolic scheme. Numerical results show that the proposed method improves the local adaptability of the subdivision process and provides better shape control than the classic uniform hyperbolic scheme.

Keywords: hyperbolic subdivision schemes; geometric modeling; computational geometry; artificial intelligence; Machine learning; curve refinement; shape optimization.

1 Introduction

Subdivision schemes are now fundamental tools in geometric modelling, computer-aided design (CAD), and computer graphics. Their main purpose is to generate smooth curves or surfaces from a discrete set of points called control polygons. The general principle is to iteratively apply refinement rules that produce a sequence of increasingly fine polygons converging to a regular boundary curve. Thanks to their algorithmic simplicity, local nature, and numerical efficiency, subdivision schemes are widely used for the representation and manipulation of complex geometric shapes in several scientific and industrial fields [10, 12, 11].

In the literature, several families of subdivision schemes have been proposed to improve the geometric properties of the curves they generate. Among the most studied approaches are polynomial, trigonometric, and hyperbolic schemes. In their classical formulation, these schemes are generally defined as uniform schemes, in which the coefficients or weights used in the refinement rules are constant and applied identically to the entire control polygon.In contrast, non-uniform schemes allow local parameters to vary along the control polygon, thereby offering more flexible geometric control [3, 7]. Several recent studies have proposed advanced variants of subdivision schemes, including non-stationary schemes and mixed formulations combining different mathematical functions [2, 5, 4, 8]. In addition, some research has introduced approaches to improve shape control using rational functions. [1].

Despite their many theoretical properties, uniform subdivision schemes have certain limitations. In particular, the use of constant global parameters or weights can limit the scheme's ability to adapt to local geometric variations in the control polygon. In real-world applications, geometric shapes may have areas of high curvature, relatively flat regions, or abrupt transitions that require more precise local control. To overcome these limitations, we propose a new artificial intelligence-based approach that transforms a uniform hyperbolic subdivision scheme into a non-uniform scheme.The main idea is to use a machine learning model that analyses the geometry of the control polygon to automatically generate local subdivision parameters. This approach aims to improve the local adaptability of the generated curves while preserving the analytical structure of the basic hyperbolic scheme.

The rest of this article is organised as follows. Section 2 presents the mathematical framework of the hyperbolic subdivision scheme and the associated algorithm. Section 3 provides an overview of existing work related to subdivision schemes and adaptive approaches. Section 4 describes the artificial intelligence-based method used to generate the local parameters of the non-uniform scheme. Section 5 presents the numerical results obtained to evaluate the performance of the proposed approach. Finally, a general conclusion is presented in the last section.

[1]Abdelmalek Essaâdi University, ENSA Tétouan, Morocco
[2]University of Tours, LIFAT EA 6300, France

Spline Orbifold Spaces

Hartmut Prautzsch[1]

Abstract

Spline orbifolds are arbitrarily smooth - open or closed - freeform splines defined over the unit sphere, the affine or hyperbolic plane of topological genus 0, 1 or higher, respectively. They are piecewise polynomial over the affine plane and piecewise rational over the sphere and the hyperbolic plane. Over the plane, they are the well-known splines over triangulations, for which we can build spline spaces (for instance by splitting triangles into micro triangles), construct bases and compute dimensions.

In this talk, I will point out that basically all we know about piecewise polynomial splines over planar triangulations can be carried over to piecewise rational orbifold splines over spherical and hyperbolic triangulations. The reason behind is that triangular rational spline orbifolds have homogeneous polynomial representations over spatial triangulations. Furthermore, I will present a piecewise rational bi-cubic C^1 element for quadrilateral orbifold splines that has no piecewise polynomial counterpart.

[1]KIT Department of Informatics, Karlsruhe Institute of Technology, Germany

GMP-X Conference on Geometry and Applied Mathematics
April 10–11, 2026 · Marrakesh, Morocco

Volumetric Decomposition for Optimized Rigid Mold Disassembly

Luca Garau[1,2] · Daniela Giorgi[2] · Luigi Malomo[2] · Gianmarco Cherchi[3] · Andrea Favilli[1,2] · Francesco Laccone[2] · Paolo Cignoni[2]

Abstract

The production of solid objects via casting is a key technology in both industrial manufacturing and traditional craftsmanship, due to its efficiency, its ability to replicate complex models, and the reusability of molds.
However, classical casting techniques are fundamentally constrained by geometric limitations: in order to allow extraction, the object's surface must typically conform to a height field.
Flexible molds can deform to accommodate undercuts, geometry features that make extraction along a single direction impossible [2], yet they suffer from material leakage, limited durability, and poor compatibility with industrial automation. Rigid mold decomposition splits the object into multiple double height field components [1], but introduces aesthetic seams and potential structural weaknesses along the joints.
In this work-in-progress, we explore an alternative strategy based on volumetric decomposition [3] to subdivide a rigid mold into multiple extractable parts. Unlike existing approaches that either modify the target geometry or generate a large number of components, our goal is to design a method that produces an optimized and structurally robust set of mold pieces. The objectives are to guarantee global disassembly, define a feasible extraction sequence, and preserve the aesthetic quality of the original design while retaining the practical advantages of rigid molds.

References

[1] T. Alderighi, L. Malomo, B. Bickel, P. Cignoni, and N. Pietroni. Volume decomposition for two-piece rigid casting. *ACM Trans. Graph.*, 40(6), Dec. 2021.

[2] T. Alderighi, L. Malomo, D. Giorgi, N. Pietroni, B. Bickel, and P. Cignoni. Metamolds: computational design of silicone molds. *ACM Trans. on Graphics - Siggraph 2018*, 37(4), August 2018.

[3] C. Araújo, D. Cabiddu, M. Attene, M. Livesu, N. Vining, and A. Sheffer. Surface2Volume: surface segmentation conforming assemblable volumetric partition. *ACM Trans. Graph.*, 38(4):80:1–80:16, 2019.

[1]Department of Computer Science, University of Pisa, Italy
[2]ISTI - CNR, Italy
[3]Department of Mathematics and Computer Science, University of Cagliari, Italy

GMP-X Conference on Geometry and Applied Mathematics
April 10–11, 2026 · Marrakesh, Morocco

Dimensionality Reduction and First-Order Riemannian Optimization: Applications in Face Recognition

Hajar Lafdili[1] · Abdeslem Hafid Bentbib[1] · Karim Kreit[1] · Oumaima Benchettou[2]

Abstract

Reducing the number of features in large datasets is a crucial step in modern data analysis, especially when dealing with high-dimensional information. High-dimensional data often contain redundant or irrelevant details, which can slow down computations and make analysis more difficult. **Dimensionality reduction** helps retain the most important information while improving computational efficiency.
In **applications** such as face recognition, data are typically represented by high-resolution images, resulting in very large feature spaces. To achieve reliable recognition, these data need to be mapped into lower-dimensional spaces that still reflect their essential structure. This often leads to constrained optimization problems that cannot be solved effectively with standard Euclidean methods.
Riemannian optimization offers a natural approach by formulating problems directly on smooth manifolds. Using geometric tools such as Riemannian metrics, gradients, and geodesic curves, optimization algorithms can operate efficiently on curved spaces.
This work covers the essential principles of Riemannian geometry and explores various optimization strategies, such as **Riemannian Gradient Descent, Riemannian Stochastic Gradient Descent, and the Riemannian Stochastic Variance Reduced Gradient Method**. These methods provide a rigorous mathematical and computational framework for **dimensionality reduction and face recognition on matrix manifolds**, particularly Grassmann and Stiefel manifolds. Accordingly, certain references are included in this presentation.

References

[1] P.-A. Absil, C. G. Baker, and K. A. Gallivan. Trust-region methods on riemannian manifolds. *Foundations of Computational Mathematics*, 7(3):303–330, 2007.

[2] P.-A. Absil, R. Mahony, and R. Sepulchre. *Optimization Algorithms on Matrix Manifolds*. Princeton University Press, 2008.

[3] R. Altmann, D. Peterseim, and T. Stykel. Riemannian newton methods for energy minimization problems of kohn–sham type. *Journal of Scientific Computing*, 101:6, 2024.

[4] Nicolas Boumal. *Optimization and Estimation on Manifolds*. PhD thesis, Université catholique de Louvain, 2015.

[5] Nicolas Boumal. *An Introduction to Optimization on Smooth Manifolds*. Cambridge University Press, 2023.

[6] Nicolas Boumal et al. Manopt: A matlab toolbox for optimization on manifolds, 2025.

[7] E. J. Candès and T. Tao. The power of convex relaxation: Near-optimal matrix completion. *IEEE Transactions on Information Theory*, 56(5):2053–2080, 2009.

[8] Yian Deng and Tingting Mu. Faster riemannian newton-type optimization by subsampling and cubic regularization. *Machine Learning*, 112:3527–3589, 2023.

[9] W. Huang and K. Wei. An extension of fast iterative shrinkage-thresholding to riemannian optimization for sparse principal component analysis, 2019. arXiv preprint.

[10] H. Kasai, H. Sato, and B. Mishra. Riemannian stochastic variance reduced gradient algorithm with retraction and vector transport, 2017. arXiv preprint.

[11] John M. Lee. *Introduction to Smooth Manifolds*. Springer, 2012.

[12] J. Nocedal and S. J. Wright. *Numerical Optimization*. Springer, 2 edition, 2006.

[13] S. Rebegoldi. *Variable metric line-search based methods for nonconvex optimization*. PhD thesis, Università degli Studi di Modena e Reggio Emilia, 2016.

[14] M. Richardson. Principal component analysis. Technical report, May 2009.

[15] J. W. Robbin and D. A. Salamon. Introduction to differential geometry, 2024. Preprint.

[16] Hiroyuki Sato. *Riemannian Optimization and Its Applications*. Springer, 2021.

[17] Loring W. Tu. *An Introduction to Manifolds*. Springer, 2011.

[18] Loring W. Tu. *Differential Geometry: Connections, Curvature, and Characteristic Classes*, volume 275 of *Graduate Texts in Mathematics*. Springer, 2017.

[1]Department of Applied Mathematics, Faculty of Sciences and Technology, Cadi Ayyad University
[2]Department of Applied Mathematics, Faculty of Sciences and Technology, Sultan Moulay Slimane University

GMP-X Conference on Geometry and Applied Mathematics
April 10–11, 2026 · Marrakesh, Morocco

Adaptive edge detection using symmetric q-derivatives: generalization of the Sobel, Prewitt, Roberts, and Canny operators.

Ranya Salouani[1] · Mohamed Lamnii[2]

Abstract

Edge detection represents a fundamental step in image processing [2], although conventional methods such as Sobel [5], Prewitt [3], Roberts [4] and Canny [1] have several limitations as sensitivity to noises or complex structures. This article introduces a generalization of these operators based on the symmetric q-derivative, a concept from differential q calculus. Through this approach, q-Sobel, q-Prewitt, q-Roberts, and q-Canny filters are formulated discretely for application to digital images. The major innovation lies in the integration of the parameter q, which offers the necessary flexibility to adjust the sensitivity of the detection, thus allowing optimization of the trade-off between localization accuracy and robustness to disturbances.

References

[1] *John Canny, A Computational Approach to Edge Detection*, IEEE Transactions on Pattern Analysis and Machine Intelligence, Vol. 8, No. 6, 1986, pp. 679-698.

[2] Rafael C. Gonzalez and Richard E. Woods, *Digital Image Processing*, Prentice Hall, 2008.

[3] J. M. S. Prewitt, *Object Enhancement and Extraction*, Picture Processing and Psychopictorics, 1970, pp. 75-149.

[4] Lawrence G. Roberts, *Machine Perception of Three-Dimensional Solids*, Optical and Electro-Optical Information Processing, 1965, pp. 159-197.

[5] Irwin Sobel, *An Isotropic* 3×3 *Image Gradient Operator*, Stanford Artificial Intelligence Project (SAIL), 1970, pp. 1-3.

[1]Department of Mathematics, Mohammed I University, Morocco.
[2]Department of Mathematics, Mohammed I University, Morocco.

GMP-X Conference on Geometry and Applied Mathematics
April 10–11, 2026 · Marrakesh, Morocco

On the concept of symmetry

A. Benroummane

Abstract

A summary reading is given on the main results concerning the following types of symmetries:

Let (M, g) be a smooth pseudo-Riemannian differential manifold with the Levi-Civita connection ∇, the Riemann curvature R and let $\mathcal{X}(M)$ be the space of vector fields on M.

1. M is called a generalized symmetric manifold (s-manifold) if each point $m \in M$ is an isolated fixed point of an isometry s_m
2. The generalized symmetric space M is said to be of order ≥ 2 if each isometry s_m is of order k (i.e, $s_m^k = id_M$ and $s_m^{k-1} \neq id_M$).
3. If $k = 2$, M is said to be globally symmetric.
4. M is locally symmetric if every point m has a neighborhood N_m in which the geodesic symmetry $s_m : N_m \longrightarrow N_m$ is an isometry, where $s_m : x \mapsto s_m(x) = \gamma_x(-1)$ such that γ_x is the geodesic curve from $m = \gamma_x(0)$ to $x = \gamma_x(1)$ for all $x \in N_m$.
5. M is said to be $k-$infinitesimally symmetric if the curvature satisfies $\nabla^{k-1}R \neq \nabla^k R = 0$ where $k \in \mathbb{N}^*$.
6. M is semi-symmetric if $R.R = 0$, that is:
$$[R(X,Y), R(Z,T)] = R(R(X,Y)Z,T) + R(Z, R(X,Y)T),$$
for all X, Y, Z, $T \in \mathcal{X}(M)$.
7. M is $H-$symmetric if $\phi^* R = R$ for all $\phi \in H$ where H is a Lie subgroup of Isometric group of M.

References

[1] [A] A. Benroummane, M. Boucetta, A. Ikemakhen, Four-dimensional homogeneous semi-symmetric Lorentzian manifolds, Differential Geometry and its Applications 56 (2018) 211-233.

[2] A. Benroummane, Four-dimensional homogeneous semi-symmetric neutral manifolds, Geometriae Dedicata, GEOM-D-00124R2(DOI.10.1007/s10711-024-00898-z)(Accepted 1-2-2024). https://arxiv.org/abs/2105.07859v2.[Maths. DG].

[3] A. Benroummane, Some Results on Semi-Symmetric Spaces, International Journal of Computational Geometry & Applications, Vol. 33, Nos. 3 & 4 (2023) 65?84.

[4] O. F. Blanco, M. Sánchez, J. M. Senovilla, Complete classification of second-order symmetric spacetimes, Journal of Physics: Conference Series 229 (2010) 012021.

[5] M. Cahen and N. Wallach, Lorentzian symmetric spaces Bull. Amer. Math. Soc.(1970) 76 585-591

[6] É. Cartan, Sur une classe remarquable d'espaces de Riemann Bull. Soc. Math. France 54, 214-264(1926).

[7] A. Haji-Badali, A. Zaeim, Semi-symmetric four dimensional neutral Lie groups. Czechoslovak Mathematical Journal, 70 (145) (2020), 393 − 410.

[8] A. J . Ledger, Espace de Rieman Symetriques Generalised, C.R. Acad. Sci . 264 (1967) 947 - 948

[9] Z. I. Szabo, Structure theorems on Riemannian manifolds satisfying $R(X,Y).R = 0$, I, the local version, J. Differential Geom. 17 (1982), 531-582.

[1]Computer Engineering & Mathematics, ENSAB, HASSAN First University, Morocco

GMP-X Conference on Geometry and Applied Mathematics
April 10–11, 2026 · Marrakesh, Morocco

Symplectic Leibniz Algebras

Abid Fatima-Ezzahrae[1] · Boucetta Mohamed[1]

Abstract

We introduce symplectic left Leibniz algebras and symplectic right Leibniz algebras as generalizations of symplectic Lie algebras. These algebras possess a left symmetric product and are Lie-admissible. We describe completely symmetric Leibniz algebras that are symplectic as both left and right Leibniz algebras. Additionally, we show that symplectic left or right Leibniz algebras can be constructed from a symplectic Lie algebra and a vector space through a method that combines the double extension process and the T^*-extension. This approach allows us to generate a broad class of examples.

References

[1] E. Barreiro and S. Benayadi, A New Approach to Leibniz Bialgebras, Algebra and Representation Theory **19** (2016) 71-101.

[2] A. M. Bloh, On a generalization of the concept of Lie algebra, Dokl. Akad. Nauk SSSR **165** (1965), 471-473.

[3] J. L. Loday, Une version non-commutative des algèbres de Lie, L'Ens. Math **39** (1993) 269-293.

[4] A. Medina, P. Revoy, Algèbres de Lie et produit scalaire invariant (French) [Lie algebras and invariant scalar products], Ann. Sci. Ecole Norm. Sup. (4) 18 3 (1985), 553-561.

[1]Cadi Ayyad University, Faculty of Sciences and Technology
[1]Cadi Ayyad University, Faculty of Sciences and Technology

GMP-X Conference on Geometry and Applied Mathematics
April 10–11, 2026 · Marrakesh, Morocco

Flat left-invariant Lorentzian metrics on almost abelian Lie groups

Ignacio Bajo[1] · Saïd Benayadi[2] · Hicham Lebzioui[3]

Abstract

Almost abelian Lie groups are those admitting a normal subgroup which is commutative and of codimension one. We determine all Lie algebras of almost abelian Lie groups admitting a left-invariant Lorentzian metric of vanishing curvature. For each of those algebras, we completely classify the set of inequivalent flat Lorentzian products.

References

[1] M. Ait Ben Haddou, M. Boucetta and H. Lebzioui, *Left-Invariant Lorentzian Flat Metrics on Lie Groups*, Journal of Lie Theory, V. 22 (2012), 269–289.

[2] A. Aubert and A. Medina, *Groupes de Lie Pseudo-Riemanniens Plats*, Tohoku Mathematical Journal, 55 (2003), 487–506.

[3] I. Bajo, S. Benayadi and H. Lebzioui, *Classification of flat Lorentzian nilpotent Lie algebras*, Bulletin of the London Mathematical Society 56 (2024), 2132–2149.

[4] O. Baues, *Prehomogeneous affine representations and flat pseudo-Riemannian manifolds*, in "Handbook of Pseudo-Riemannian Geometry and Supersymmetry", V. Cortés (ed.), IRMA Lectures in Mathematics and Theoretical Physics 16, EMS, ZÃ¼rich (2010), 731–817.

[5] M. Boucetta and H. Lebzioui, *On Flat Pseudo-Euclidean Nilpotent Lie Algebras*, Journal of Algebra 537 (2019), 459–477.

[6] M. Boucetta and H. Lebzioui, *Flat Nonunimodular Lorentzian Lie Algebras*, Communications in Algebra, 44 (2016), Issue 10, 4185–4195.

[7] M. Guédiri, *On the nonexistence of closed timelike geodesics in flat lorentz 2-step nilmanifolds*, Transactions of the American Mathematical Society, 355 (2003), 775–786.

[8] F. Grunewald and G. Margulis, *Transitive and quasitransitive actions of affine groups preserving a generalized Lorentz-structure*, Journal of Geometry and Physics 5, no. 4 (1988), 493–531.

[9] J. Helmstetter, *Radical d'une algèbre symétrique à gauche*, Annales de l'Institut Fourier, Tome 29 (1979), no. 4, 17-35.

[10] H. Lebzioui, *Flat left-invariant pseudo-Riemannian metrics on unimodular Lie groups*, Proceedings of the American Mathematical Society, Volume 148, Number 4 (2020), 1723–1730.

[11] J. Milnor, *Curvature of left invariant metrics on Lie Groups*, Advances in Mathematics, 21 (1976), 293–329.

[12] K. Nomizu, *Left-invariant Lorentz metrics on Lie groups*, Osaka Journal of Mathematics, Volume 16, Number 1 (1979), 143–150.

[13] D. Segal, *The structure of complete left-symmetric algebras*, Mathematische Annalen, 293 (1992), no. 3, 569–578.

[1]Depto. Matemática Aplicada II, Universidade de Vigo, Campus Marcosende, 36310 Vigo, Spain.
[2]Labor. IECL, CNRS-UMR 7502, UFR MIM, Université de Lorraine, 3 rue Augustin Fresnel BP 45112, F-57073 Metz Cedex 03, France.
[3]École Supérieure de Technologie Khénifra, Université Sultan Moulay Slimane, B.P: 170, Khénifra, Morocco.

GMP-X Conference on Geometry and Applied Mathematics
April 10–11, 2026 · Marrakesh, Morocco

NATURAL RICCI SOLITONS ON TANGENT AND UNIT TANGENT BUNDLES

M. T. K Abbassi[1] · Nora Amri[1]

Abstract

Considering pseudo-Riemannian g-natural metrics on tangent bundles, we prove that the condition of being Ricci soliton is hereditary in the sense that a Ricci soliton structure on the tangent bundle gives rise to a Ricci soliton structure on the base manifold. When unit tangent bundles over a constant curvature Riemannian manifold are endowed with pseudo-Riemannian Kaluza-Klein type metric, we give a classification of Ricci soliton structures whose potential vector fields are fiber-preserving, inferring the existence of some of them which are non Einstein.

References

[1] M. T. K. Abbassi, N. Amri, *On conformal vector field on unit tangent sphere bundles with g-natural metrics*, to appear in Czech. Math. J.

[2] M. T. K. Abbassi, N. Amri, G. Calvaruso, *Kaluza-Klein type Ricci Solitons on Unit Tangent Sphere Bundles*, Diff. Geom. Appl. 59 (2018), 184–203.

[3] M. T. K. Abbassi, N. Amri, *Natural Ricci Solitons on tangent and unit tangent bundles*, Journal of Mathematical Physics, Analysis, Geometry.

[1]Department of mathematics, Sidi Mohammed Ben Abdellah university, faculty of science, Fez, Morocco

GMP-X Conference on Geometry and Applied Mathematics
April 10–11, 2026 · Marrakesh, Morocco

The volume of a Vector field on a Riemmanian manifold

M. T. K Abbassi[1] · Nora Amri[1] · Oumaima Bradaai[1]

Abstract

Let (M, g) be a Riemannian manifold. We introduce the volume functional defined on the space of smooth sections of the tangent bundle equipped with the g-natural metric, and give the first variation formula with the aim of studying critical points of this functional, reducing to the case of parallel and unit vector fields.

References

[1] M. T. K. Abbassi, *Note on the classification Theorems of g-natural metrics on the tangent bundle of a Riemannian manifold* (M, g), Comment. Math. Univ. Carolinae, 45(4): 591–596, 2004.

[2] O. Gil-Medrano, *The volume of vector fields on Riemannian manifolds: main results and open problems*, Lecture Notes in Math., Springer, 2023.

[1]Department of mathematics, Sidi Mohammed Ben Abdellah university, faculty of science, Fez, Morocco

Short Papers

GMP-X Conference on Geometry and Applied Mathematics
April 10–11, 2026 · Marrakesh, Morocco

Positive Hyperbolic Barycentric Coordinates for Non-Convex Polygons

Alaa Eddine Bensad[1] · Aziz Ikemakhen[1]

Abstract

This paper presents a method for computing barycentric coordinates for non-convex polygonal shapes on the hyperbolic plane. The proposed approach ensures positivity and smoothness coordinates, making it suitable for applications such as hyperbolic image deformation. The method is based on associating points inside a hyperbolic polygon with a planar polygon inscribed in the Euclidean unit circle, allowing hyperbolic coordinates to be derived from their planar counterparts. Experimental results demonstrate the effectiveness of the proposed coordinates in deformation tasks on hyperbolic surfaces, highlighting their potential for hyperbolic geometry processing.

1 Introduction

Barycentric coordinates provide a unique way of representing a point's location within a fixed polygon as an affine combination of the polygon's vertices. They play a key role in computer graphics and geometry processing, with applications in finite element analysis, interpolation, parameterization, shape morphing, and mesh deformation. However, barycentric coordinates are not unique in the case of planar polygons with more than three vertices. This has led to the development of several families of generalized barycentric coordinates. Each type offers distinct advantages depending on desired properties and applications, as detailed in [14, 4, 5, 10, 11, 9, 7].

In the same way, surface barycentric coordinates offer a distinct approach for locating points on surfaces relative to geodesic polygons. Rustamov [13] studied barycentric coordinates on surfaces using the Riemannian center of mass and the exponential map. On the hyperbolic plane, the study of generalized barycentric coordinates was recently done by Bensad et al. [1], suggesting promising applications in Network Analysis, Hyperbolic Deep Neural Networks (HDNNs), and hyperbolic game design.

2 Related work

Planar barycentric coordinates have generated significant interest due to their applications in computational geometry, computer graphics, and finite element methods. Many constructions of barycentric coordinates have been developed, such as Wachspress coordinates [14], discrete harmonic coordinates [4], mean value coordinates [5], metric coordinates [10], Gordon-Wixom [11], Poisson [9], and other coordinates [7, 6].

However, research on surface barycentric coordinates remains less comprehensive. Rustamov [13] explored their definition on general surfaces using the Riemannian center of mass and the exponential map, but did not provide explicit formulas for their computation. On the sphere $\mathbb{S}^2$, progress has been made to efficiently compute barycentric coordinates using tangent spaces [8, 2]. Meanwhile Bensad et al. [1] introduced the concept of generalized hyperbolic barycentric coordinates using hyperbolic gnomonic projection. By combining hyperbolic triangles, their gnomonic projections, and the relationship between Euclidean and hyperbolic trigonometry, expressions for hyperbolic Wachspress, hyperbolic mean value, and hyperbolic discrete harmonic coordinates were thus derived.

3 Contributions

This paper proposes a method for computing positive barycentric coordinates relative to hyperbolic polygons. These coordinates offer two key advantages: guaranteed positivity and the ability to represent interior points of non-convex polygons. We rely solely on the familiar tools of hyperbolic trigonometry and the Euclidean unit circle (Section 5).

To demonstrate the advantages of these hyperbolic coordinates, we explore concrete examples of image warping on the hyperbolic plane and its model the Poincaré disc. We pay particular attention to non-convex shapes where our approach shines (Section 6).

4 Hyperbolic geometry and hyperbolic barycentric coordinates

This section gives an overview of hyperbolic geometry on the hyperbolic plane and the Poincaré disc, as well as the construction of hyperbolic barycentric coordinates.

[1]Department of Mathematics, Faculty of Science and Technology, Cadi Ayyad University, Marrakesh, Morocco

3. Let $v \in \mathbb{H}$ be an arbitrary point within P (see Figure 1b). We call *hyperbolic barycentric coordinates* of v with respect to P any set of real coefficients $(\lambda_1, \ldots, \lambda_n)$, depending on the vertices of P and on v, that satisfy

$$v = \sum_{i=1}^{n} \lambda_i v_i, \quad \text{with} \quad \sum_{i=1}^{n} \lambda_i \leq 1.$$

The standard approach for computing hyperbolic barycentric coordinates of v involves a two-step process. First, the hyperbolic polygon P is projected onto the tangent plane $T_v\mathbb{H}$ at v, resulting in a flat polygon $\hat{P}$. Bensad et al. [1] use the gnomonic projection to perform this step. Then the hyperbolic coordinates are deduced from standard flat barycentric coordinates of v with respect to $\hat{P}$, via the equation

$$\lambda_i(v) = \frac{1}{\cosh(\theta_i)} \hat{\lambda}_i(v), \quad i = 1, \ldots, n,$$

where $\hat{\lambda}_i(v)$ are the planar barycentric coordinates of v with respect to $\hat{P}$ and $\theta_i := d_{\mathbb{H}}(v, v_i)$.
In particular, this approach yields the expressions of:

- Hyperbolic mean value coordinates

$$\lambda_i = \frac{\omega_i}{\sum_{j=1}^{n} \coth(\theta_j) \left(\tan(\frac{\alpha_{j-1}}{2}) + \tan(\frac{\alpha_j}{2}) \right)}, \quad \text{where} \quad \omega_i = \frac{\tan(\frac{\alpha_{i-1}}{2}) + \tan(\frac{\alpha_i}{2})}{\sinh(\theta_i)}. \tag{2}$$

α_i are the hyperbolic angles denoted in Figure 1b.

While hyperbolic mean value coordinates (HMVC) are a valuable tool in hyperbolic geometry processing, they only guarantee positive values inside the kernel of a star-shaped geodesic polygon. The positivity property fails for non-convex polygons, where negative values appear for some interior points. To address this limitation, we introduce a method that ensures positive coordinates even for non-convex polygons.

5 Positive hyperbolic barycentric coordinates

Let $P = [v_1, \ldots, v_n]$ be a hyperbolic polygon on $\mathbb{H}$, and v a point in the interior of P (see Figure 1b). Our construction of positive hyperbolic barycentric coordinates is based on the following proposition:

Proposition 2. *Let*

$$\hat{v}_i := \frac{1}{\sinh(\theta_i)} v_i - \coth(\theta_i) v, \quad i = 1, \ldots n, \tag{3}$$

where $\theta_i := d_{\mathbb{H}}(v_i, v)$. We have:

a) $\langle \hat{v}_i, v \rangle_L = 0$, which implies $\hat{v}_i$ lies in the orthogonal vector space to v with respect to the Lorentzian product.

b) $\langle \hat{v}_i, \hat{v}_i \rangle_L = 1$.

c) If $v = \Omega := (0, 0, 1)$, then the polygon $\hat{P} := [\hat{v}_1, \ldots, \hat{v}_n]$ is inscribed in the unit Euclidean circle C_o (centered at the origin o).

Proof. a) From (3), we get

$$v_i := \cosh(\theta_i) v + \sinh(\theta_i) \hat{v}_i, \quad \text{(see Figure 2b)}.$$

Furthermore, $\langle v, v \rangle_L = -1$, and from (1), we obtain

$$\langle \hat{v}_i, v \rangle_L = \frac{1}{\sinh(\theta_i)} \langle v_i, v \rangle_L - \coth(\theta_i) \langle v, v \rangle_L = -\frac{\cosh(\theta_i)}{\sinh(\theta_i)} + \coth(\theta_i) = 0.$$

b)

$$\langle \hat{v}_i, \hat{v}_i \rangle_L = \frac{1}{\sinh^2(\theta_i)} \langle v_i, v_i \rangle_L - 2 \frac{\coth(\theta_i)}{\sinh(\theta_i)} \langle v_i, v \rangle_L + \coth^2(\theta_i) \langle v, v \rangle_L = \frac{-1 + \cosh^2(\theta_i)}{\sinh^2(\theta_i)} = 1.$$

c) For $v = \Omega := (0, 0, 1)$, $\langle \hat{v}_i(x_i, y_i, z_i),\ \Omega \rangle_L = z_i = 0$, then $\langle \hat{v}_i, \hat{v}_i \rangle_L = x_i^2 + y_i^2 = 1$. Which proves $\hat{P}$ is inscribed in the unit Euclidean circle on the xy-plane.

□

To compute positive hyperbolic coordinates λ_i of v with respect to P, we start by treating the special case of $v = \Omega$ through a multi-step process of planar projection, midpoint averaging and re-scaling. Then, we generalize this process to any point v on the hyperbolic plane $\mathbb{H}$ using Lorentz transformations.

5.1 $v = \Omega$

In order to construct positive hyperbolic coordinates λ_i of Ω with respect to P, we first associate to P a planar polygon denoted $\hat{P} = [\hat{v}_1, \ldots, \hat{v}_n]$, such that the origin $o = (0, 0, 0)$ lies in the interior of $\hat{P}$. We then iteratively apply midpoint averaging plus re-scaling to the vertices of $\hat{P}$ until we get a cyclic convex polygon $\tilde{P}$, for the purpose of determining positive planar coordinates $\hat{\lambda}_i$ of the origin o with regard to $\hat{P}$. Finally, from $\hat{\lambda}_i$, we derive λ_i positive hyperbolic coordinates of Ω.

constitute a set of positive hyperbolic barycentric coordinates of Ω with respect to P, where $\hat{\lambda}_i$ are positive planar barycentric coordinates of the origin o with respect to $\hat{P}$, and θ_i the hyperbolic distance between Ω and v_i.

Proof. We have

$$\sum_{i=1}^{n} \hat{\lambda}_i \hat{v}_i = o. \tag{5}$$

Substituting (3) into (5) for $v = \Omega$, we get

$$\Omega = \sum_{i=1}^{n} \lambda_i v_i, \text{ with } \lambda_i = \frac{\hat{\lambda}_i}{\sinh(\theta_i) \sum_{j=1}^{n} \hat{\lambda}_j \coth(\theta_j)}. \tag{6}$$

□

5.2 General case $v \in \mathbb{H}$

Let $v \in \mathbb{H}$. Based on Theorem 1, there exists a Riemannian isometry of $\mathbb{H}$ that extends to a Lorentz transformation of $\mathbb{R}^3$, denoted A, that sends v to Ω. This translates to $Av = \Omega$. Accordingly, we generalize the process for computing positive hyperbolic coordinates of Ω (Subsection 5.1) to compute positive hyperbolic coordinates of any point v in the interior of polygon P, by noticing that

$$\sum_{i=1}^{n} \lambda_i v_i = v \Longleftrightarrow \sum_{i=1}^{n} \lambda_i Av_i = Av = \Omega. \tag{7}$$

Consequently, we take $\lambda_i(v,P)$, positive hyperbolic coordinates of v with respect to P, to be $\lambda_i(\Omega, AP)$ the positive hyperbolic coordinates of Ω, obtained from (6), with respect to the polygon $AP = [Av_1, \ldots, Av_n]$.

$$\lambda_i(v,P) := \lambda_i(\Omega, AP), \qquad \text{for} \quad i = 1, \ldots, n. \tag{8}$$

Furthermore, equation (3) for $v = \Omega$ and the polygon $AP = [Av_1, \ldots, Av_n]$ yields the planar points

$$\hat{\Omega}_i := \frac{1}{\sinh(\theta_i)} Av_i - \coth(\theta_i)\Omega. \tag{9}$$

By applying A^{-1} to both sides of (9), we get

$$A^{-1}\hat{\Omega}_i = \frac{1}{\sinh(\theta_i)} v_i - \coth(\theta_i) A^{-1}\Omega = \frac{1}{\sinh(\theta_i)} v_i - \coth(\theta_i) v = \hat{v}_i. \qquad \text{(as defined in Proposition 2)}$$

Subsequently, if $\hat{P} = [\hat{v}_1, \ldots, \hat{v}_n]$ is the polygon formed by the vertices $\hat{v}_i$, and $\hat{\lambda}_i$ are positive planar coordinates of the origin o with respect to $\hat{P}$, it follows that

$$\sum_{i=1}^{n} \hat{\lambda}_i \hat{\Omega}_i = \sum_{i=1}^{n} \hat{\lambda}_i (A\hat{v}_i) = A\left(\sum_{i=1}^{n} \hat{\lambda}_i \hat{v}_i \right) = Ao = o. \tag{10}$$

Equation (10) establishes that any planar coordinates $\hat{\lambda}_i$ of the origin o with respect to $\hat{P} = [\hat{v}_1, \ldots, \hat{v}_n]$ are also planar coordinates of the origin with respect to $A\hat{P} = [\hat{\Omega}_1, \ldots, \hat{\Omega}_n]$. We take

$$\hat{\lambda}_i(o, A\hat{P}) := \hat{\lambda}_i(o, \hat{P}), \qquad \text{for} \quad i = 1, \ldots, n. \tag{11}$$

Based on (6), (8), (11) and the fact that A preserves distances, we avoid computing $\lambda_i(\Omega, AP)$ and $\hat{\lambda}_i(o, A\hat{P})$ to compute $\lambda_i(v,P)$, since both require determining A explicitly. Instead, we directly compute $\hat{\lambda}_i(o,\hat{P})$, the positive planar coordinates obtained via the iterative smoothing process (Subsection 5.1.2) applied to vertices $\hat{v}_i$. Then, we derive $\lambda_i(v,P)$ by substitution in (6).

6 Applications

This section evaluates the effectiveness of positive hyperbolic barycentric coordinates for image deformation. This is achieved through illustrative examples on the hyperbolic plane $\mathbb{H}$ and the Poincaré disc $\mathbb{D}$, by comparison with mean value coordinates.

6.1 Hyperbolic image deformations

To perform image deformations on the hyperbolic plane and the Poincaré disc using barycentric mapping, we need to compute a pixel's barycentric coordinates with respect to a hyperbolic polygon.

Definition 2. Let $P = [v_1, \ldots, v_n]$ be a source polygon, and $P' = [v'_1, \ldots, v'_n]$ a target polygon in $\mathbb{H}$. We denote by $\mathring{P}$ (resp. $\mathring{P}'$) the surface in $\mathbb{H}$ enclosed by P (resp. P'). The barycentric mapping $f : \mathring{P} \longrightarrow \mathring{P}'$ is defined as

$$f(v) := \frac{v'}{\sqrt{-\langle v', v' \rangle_L}},$$

where $v' := \sum_{i=1}^{n} \lambda_i(v) v'_i$, and $\lambda_i(v)$ are hyperbolic barycentric coordinates of v with respect to P.

Barycentric mapping is direct on the hyperbolic plane, but requires the Riemannian isometry Ψ, which maps points from $\mathbb{H}$ to $\mathbb{D}$, for the Poincaré disc.

Proposition 4. *[1] Let $U = [u_1, \dots, u_n]$ be a hyperbolic polygon in $\mathbb{D}$, and u a point inside U (see Figure 1c). Let $v := \Psi^{-1}(u) \in \mathbb{H}$. If $(\lambda_i(v))_{i=1,\dots,n}$ denote hyperbolic barycentric coordinates of v with respect to $\Psi^{-1}(U)$, then barycentric coordinates of u with respect to U can be expressed as*

$$\phi_i(u) := \frac{1-\|u\|^2}{1-\|u_i\|^2}\,\lambda_i(v), \qquad i = 1, \dots, n.$$

Consequently, the barycentric mapping, $f : \mathring{U} \longrightarrow \mathring{Q}$, between a source polygon $U = [u_1, \dots, u_n]$ and a target polygon $Q = [q_1, \dots, q_n]$ in $\mathbb{D}$ is given by

$$f(u) = \sum_{i=1}^{n} \phi_i(u) q_i,$$

where $\phi_i(u)$ are hyperbolic barycentric coordinates of u with respect to U, satisfying $\sum_{i=1}^{n} \phi_i(u) \leq 1$. This mapping is used to deform an image originally residing within U to a corresponding image within Q.

Figure 4 showcases the application of barycentric mappings for image deformation on the hyperbolic plane and the Poincaré disc. It displays three columns:

- Left Column: input images placed onto the Poincaré disc or the hyperbolic plane.
- Middle Column: deformations by barycentric mmapping with hyperbolic mean value coordinates (HMVC).
- Right Column: deformations by barycentric mapping with positive hyperbolic coordinates (PHC).

Each image is inscribed within a hyperbolic polygon defined by vertices $p_1, ..., p_n$. Both HMVC and PHC of pixels are computed with respect to this polygon. The images are subsequently deformed by replacing some initial vertices with new ones, $\hat{p}_1, ..., \hat{p}_n$, and applying the corresponding barycentric mapping.
Key Observations: Both barycentric mappings produce deformed images that fit within the new polygon, and the deformations become less pronounced away from the edges. However, the choice of barycentric coordinates used and their sign lead to distinct visual outcomes:

- HMVC produce disfigured and damaged images with jagged edges and irregular shapes in some areas. Notably, small changes to few adjacent vertices distort large portions of the images.
- PHC produce deformed images with smoother edges, and a better preservation of shapes illustrated in the images. Furthermore, there are less artefacts in areas further away from the modified vertices.

7 Conclusion

This work introduces a method for computing positive hyperbolic barycentric coordinates with respect to non-convex polygons, on the hyperbolic plane and its model the Poincaré disc. These coordinates are advantageous for image deformation, where better results are obtained in comparison with standard hyperbolic barycentric coordinates. A natural progression is to explore computing positive barycentric coordinates on other homogeneous Riemannian surfaces. Another future direction could involve computing positive barycentric coordinates on mesh surfaces.

References

[1] A. e. Bensad and A. Ikemakhen. Hyperbolic barycentric coordinates and applications. *Computer Aided Geometric Design*, page 102086, 2022.

[2] A. e. Bensad and A. Ikemakhen. A general construction of spherical barycentric coordinates and applications. *Journal of Computational and Applied Mathematics*, 422(4):114945, 2023.

[3] C. Deng, Q. Chang, and K. Hormann. Iterative coordinates. *Computer Aided Geometric Design*, 79:101861, 2020.

[4] M. Eck, T. DeRose, T. Duchamp, H. Hoppe, M. Lounsbery, and W. Stuetzle. Multiresolution analysis of arbitrary meshes. In *Proceedings of the 22nd annual conference on Computer graphics and interactive techniques*, pages 173–182, 1995.

[5] M. S. Floater. Mean value coordinates. *Computer aided geometric design*, 20(1):19–27, 2003.

[6] M. S. Floater. Generalized barycentric coordinates and applications. *Acta Numerica*, 24:161–214, 2015.

[7] M. S. Floater, K. Hormann, and G. Kós. A general construction of barycentric coordinates over convex polygons. *advances in computational mathematics*, 24(1-4):311–331, 2006.

[8] T. Langer, A. Belyaev, and H.-P. Seidel. Spherical barycentric coordinates. In *Symposium on Geometry Processing*, pages 81–88, 2006.

[9] X.-Y. Li and S.-M. Hu. Poisson coordinates. *IEEE Transactions on visualization and computer graphics*, 19(2):344–352, 2012.

[10] E. A. Malsch, J. J. Lin, and G. Dasgupta. Smooth two-dimensional interpolations: a recipe for all polygons. *Journal of Graphics Tools*, 10(2):27–39, 2005.

[11] J. Manson, K. Li, and S. Schaefer. Positive gordon–wixom coordinates. *Computer-Aided Design*, 43(11):1422–1426, 2011.

[12] J. Ratcliffe. Foundations of hyperbolic manifolds. *Graduate Texts in Mathematics/Springer-Verlag*, 149, 1994.

[13] R. M. Rustamov. Barycentric coordinates on surfaces. In *Computer Graphics Forum*, volume 29, pages 1507–1516. Wiley Online Library, 2010.

[14] E. L. Wachspress and W. EL. A rational finite element basis. 1975.

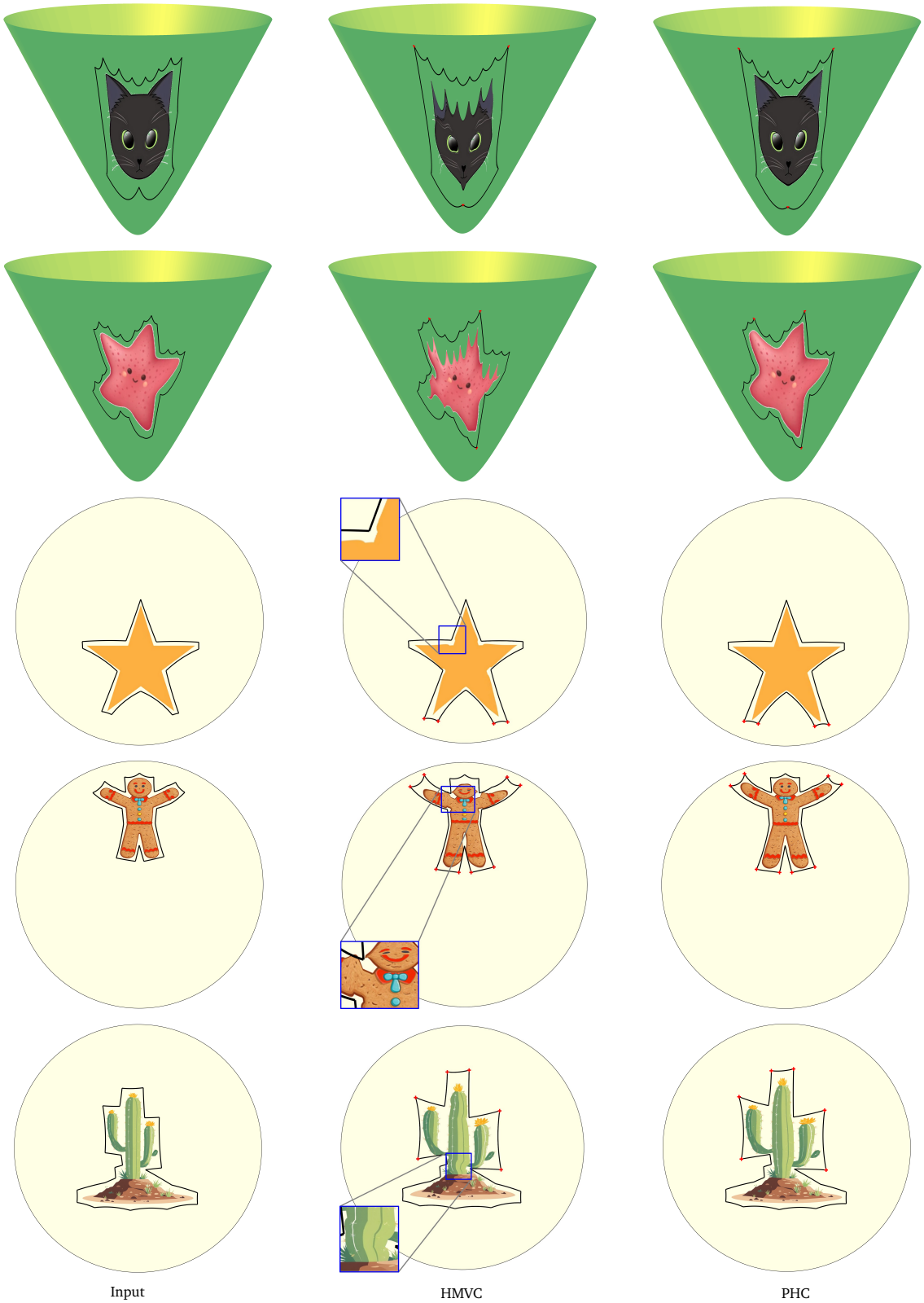

Figure 4: Comparison of image deformations using hyperbolic mean value coordinates (HMVC) and positive hyperbolic ones (PHC) on the hyperbolic plane and the Poincaré disc.

GMP-X Conference on Geometry and Applied Mathematics
April 10–11, 2026 · Marrakesh, Morocco

A learning-assisted algorithmic framework for constructing a generalized Voronoi graph representation in grid space

J. Antony[1,3] · G. James[2] · J.S. Jose[2] · A. Aswinkesh[2] · E. Baiju[2] · R. Muthuganapathy[1]

Abstract

In this work, we propose a learning assisted algorithmic framework for constructing a proximity graph representation of a generalized Voronoi diagram (GVD) of general shapes modeled as a binary occupancy grid. Traditional distance transform-based skeletonization methods typically employed for Voronoi pixel extraction are found to be reliable only for convex polygonal shapes with linear boundaries. For general shapes with concavities, they often produce artifacts and inaccurate Voronoi boundaries. Although Voronoi diagrams for general shapes can be constructed by computing distance transforms separately for each shape and then integrating the results, this approach is computationally inefficient and scales poorly with increasing object count and grid resolution. To overcome these limitations, we leverage deep learning as an efficient, parallel alternative to replace the traditional methods. A curated dataset, VoroPixelSet, is built from synthetically generated object maps and their corresponding Voronoi-pixel maps. This dataset is used to train the VoroPixelNet, a DeeplabV3 based model for Voronoi pixel predictions. Comparative results show that the proposed model inference runs significantly faster than the per object distance transform-based method. Moreover, the Voronoi pixel predictions by the model are consistent and artifact-free. Building on these predictions, we connect the relevant Voronoi pixels and prune out the rest to build VoroConnect, a sparse, topologically consistent proximity graph representing the Voronoi Diagram. This resulting graph can support diverse downstream applications such as path planning, computer vision, geographical information systems, game development, etc. We demonstrate its efficacy in a path planning scenario, where it enables the computation of safe and shortest paths through complex environments. The results demonstrate the effectiveness of integrating geometric modeling principles with modern learning-driven and parallel inference techniques.

1 Introduction

Geometric modeling is a fundamental area of computational geometry that deals with problems such as the computation of convex hull (CH), Delaunay triangulations, and Voronoi diagrams. These problems form the basis of numerous applications in computer graphics, computer vision, robotics, geographic information systems (GIS), reverse engineering, image processing, etc.

The Voronoi diagram has been extensively studied due to its wide range of applications in computational geometry and computer graphics[4, 13]; A closely related concept, the distance transform [17], was introduced in image processing. It operates on a binary image and generates a distance map, where pixels labeled 0 serve as seed points and pixels labeled 1 form the background. Each pixel in the resulting map is assigned a real value representing its minimum distance to the nearest seed point.

In practical scenarios, geometric data is increasingly obtained in structured forms such as images, raster maps, and voxelized point clouds, particularly in domains including medical imaging, remote sensing, and autonomous navigation. Moreover, in many downstream applications, converting point cloud data into pixel or voxel-based representations simplifies neighborhood computation and spatial analysis. [8, 14].

Binary occupancy grid is such a structured representation in 2D widely used for spatial modeling, including obstacle maps for path planning, robotic mapping and localization, and GIS-based spatial analysis.

A *binary occupancy grid* is a fundamental spatial representation used to model two-dimensional environments. Each cell in the grid encodes whether a specific location in the workspace is free or occupied by an object. Formally, the occupancy grid can be expressed as a function

$$G(x,y) = \begin{cases} 1, & \text{if } (x,y) \in \text{O (occupied cell)}, \\ 0, & \text{if } (x,y) \in \text{F (free space)}. \end{cases}$$

where $(x,y) \in \mathbb{R}^2$, O denotes the set of object pixels, and F represents the free-space pixels.

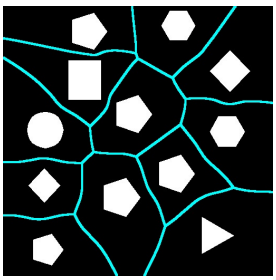

Figure 1: Binary Occupancy Grid and its Voronoi pixels in cyan color

The *Generalized Voronoi Diagram (GVD) representation* of a binary occupancy grid partitions the free space F into regions according to their proximity to the nearest object

[1]Advanced Geometric Computing Lab, Department of Engineering Design, Indian Institute of Technology Madras, Chennai-600036, India
[2]Department of Information Technology, Amal Jyothi College of Engineering, Kanjirappally, Kottayam-686518, Kerala India
[3]Division of Artificial intelligence and Machine Learning, Karunya Institute of Technology and Sciences, Karunya Nagar, Coimbatore-641114, Tamil Nadu, India

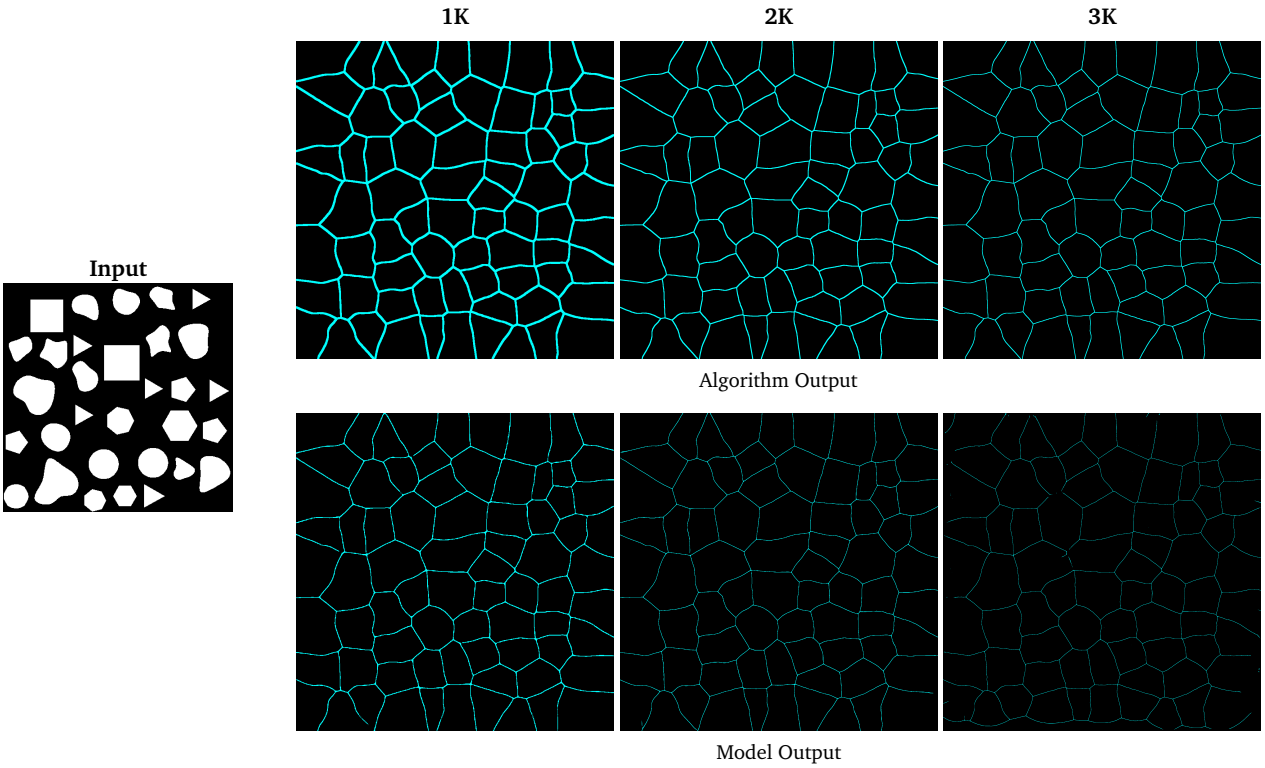

Figure 8: Qualitative comparison of algorithmic and learning-assisted Voronoi extraction across increasing grid resolutions.

[6] I. Demir, C. Hahn, K. Leonard, G. Morin, D. Rahbani, A. Panotopoulou, A. Fondevilla, E. Balashova, B. Durix, and A. Kortylewski. Skelneton 2019: Dataset and challenge on deep learning for geometric shape understanding. In *Proceedings of the IEEE/CVF conference on computer vision and pattern recognition workshops*, pages 0–0, 2019.

[7] J. C. Elizondo-Leal, G. Ramírez-Torres, J. H. Barrón-Zambrano, A. Díaz-Manríquez, M. Nuño-Maganda, and V. P. Saldivar-Alonso. Parallel Raster Scan for Euclidean Distance Transform. *Symmetry*, 12:1808, 2020.

[8] M. Gouda, Z. Pawliuk, J. Mirza, and K. El-Basyouny. Using convex hulls with octree/voxel representations of point clouds to assess road and roadside geometric design for automated vehicles. *Automation in Construction*, 154:104967, 2023.

[9] I. Hanniel, M. Ramanathan, G. Elber, and M.-S. Kim. Precise voronoi cell extraction of free-form planar piecewise c1-continuous closed rational curves. *International Journal of Computational Geometry & Applications*, 17(05):453–486, 2007.

[10] X. Hou, P. Chen, and H. Gu. Lm-deeplabv3+: A lightweight image segmentation algorithm based on multi-scale feature interaction. *Applied Sciences*, 14:1558, 02 2024.

[11] H. Moulinec. A simple and fast algorithm for computing discrete voronoi, johnson-mehl or laguerre diagrams of points. *Advances in Engineering Software*, 170:103150, 2022.

[12] N. H. Nguyen. U-net based skeletonization and bag of tricks. In *Proceedings of the IEEE/CVF International Conference on Computer Vision*, pages 2105–2109, 2021.

[13] A. Okabe, B. Boots, and K. Sugihara. Spatial tessellations: Concepts and applications of voronoi diagrams. pages I–X, 1–532, 1995.

[14] F. Poux and R. Billen. Voxel-based 3D point cloud semantic segmentation: Unsupervised geometric and relationship featuring vs deep learning methods. *ISPRS International Journal of Geo-Information*, 8(5), 2019.

[15] G. Rong and T. Tan. Jump flooding in gpu with applications to voronoi diagram and distance transform. pages 109–116, 2006.

[16] G. Rong and T. Tan. Variants of jump flooding algorithm for computing discrete voronoi diagrams. *4th International Symposium on Voronoi Diagrams in Science and Engineering (ISVD 2007)*, pages 176–181, 2007.

[17] A. Rosenfeld and J. Pfaltz. Distance functions on digital pictures. *Pattern Recognit.*, 1:33–61, 1968.

[18] L. Santos, A. Aguiar, F. Santos, A. Valente, and M. Petry. Occupancy grid and topological maps extraction from satellite images for path planning in agricultural robots. *Robotics*, 9:77, 2020.

[19] J.-K. Seong, E. Cohen, and G. Elber. Voronoi diagram computations for planar nurbs curves. In *Proceedings of the 2008 ACM symposium on Solid and physical modeling*, SPM '08, pages 67–77, New York, NY, USA, 2008. ACM.

[20] B. R. Sundar, M. K. Mukundan, and R. Muthuganapathy. A unified approach towards computing Voronoi diagram, medial axis, Delaunay graph and α-hull of planar closed curves using touching discs. *Computers & Graphics*, 89:131 – 143, 2020.

[21] B. Wang, Q. Wang, and J. Li. Lecture notes in computer science: Research on hybrid grid algorithm of voronoi diagram. 17:03005, 2018.

GMP-X Conference on Geometry and Applied Mathematics
April 10–11, 2026 · Marrakesh, Morocco

Projection-Based Structural Element Extraction from Point Clouds

Diana Marin[1] · Julia Reisinger[2] · Peter Kán[1] · Hannes Kaufmann[1]

Abstract

Extracting structural elements from building-scale point clouds is essential for structural assessment, yet remains difficult in industrial environments due to clutter, occlusions, varying density, and missing faces. We propose a fast extraction pipeline that identifies axis-aligned structural elements through orthogonal projections and 2D histograms, and groups peaks into structural candidates via graph-based clustering. The key parameters operate on an explicit histogram representation, making threshold selection visually interpretable for rapid expert iteration. Our method enables rapid conversion of cluttered scans into simulation-oriented structural primitives suitable for downstream structural analysis workflows.

1 Introduction

Industrial buildings represent a large fraction of the existing built environment and are increasingly targeted for adaptive reuse, modernization, and vertical extension. A recurring bottleneck in these workflows is structural assessment: while modern acquisition pipelines, such as photogrammetry, can deliver dense 3D point clouds of entire buildings, structural simulation and verification still rely on analytical models (e.g., beam-and-column skeletons) that are typically created manually. This manual model-building is time-consuming, requires expert knowledge, and is especially error-prone in large facilities where the load-bearing system is embedded in cluttered scenes containing machinery, piping, façades, and partition walls.

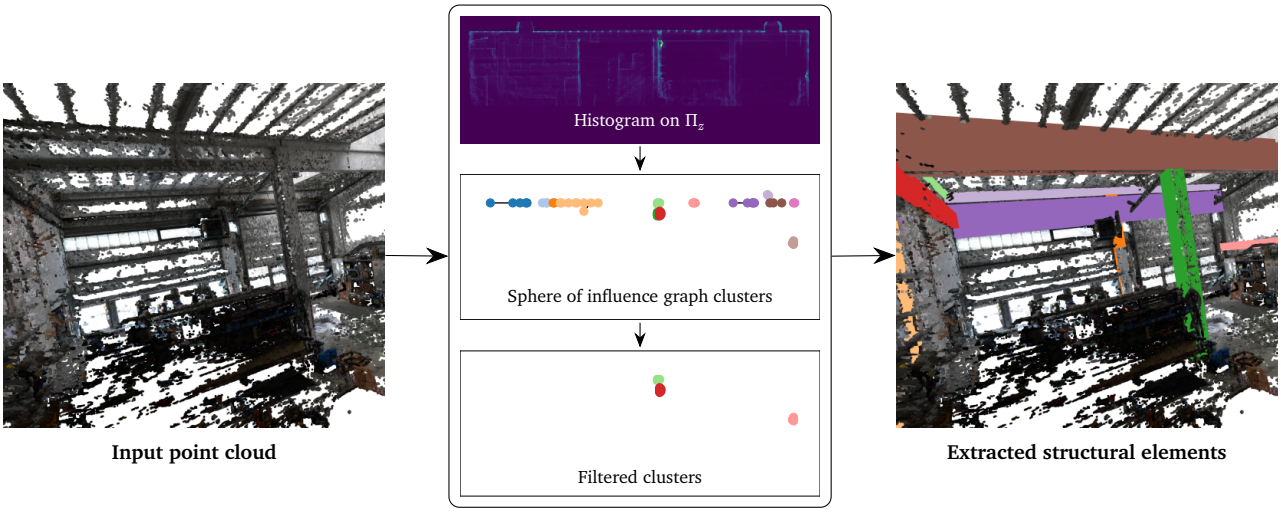

Figure 1: We are able to extract structural elements from noisy point clo lustrial buildings, through 2D projections and peak clustering in the lower-dimensional space. The histogram values correspond to FEW MANY points in each bin. The dense horizontal lines present at the top of the scanned scene are not structural, and hence, are not detected by our method, showcasing the resilience of our approach.

Most scan-based reconstruction pipelines aim at modelling the entire scene (e.g., Scan to Building Information Model) or at generating volumetric/mesh representations suitable for general finite element meshing. For structural engineering tasks on industrial halls, however, the relevant output is often a selective structural abstraction: a set of columns and beams with correct connectivity and geometric parameters that can be imported directly into structural analysis software. The presence of occlusions, missing faces, and strong non-structural geometry makes this selective extraction substantially more difficult than reconstruction from clean scans of isolated structural components.

We introduce a fast, projection-driven pipeline for automatic extraction of axis-aligned beams and columns directly from full building point clouds - Figure 1. The method leverages the observation that structural elements induce strong axis-aligned density signatures under orthogonal projection, and converts the 3D extraction problem into lightweight 2D projection aggregation

[1]TU Wien Institute of Visual Computing and Human-Centered Technology, Vienna, Austria
[2]TU Wien Institute of Building and Industrial Construction, Vienna, Austria

followed by robust lifting back to 3D. Key parameters act on an explicit and inspectable histogram representation, making threshold choice visually interpretable for rapid expert iteration. Our main contributions are:

1. Projection-histogram peak detection to identify candidate structural elements from dense building scans, replacing expensive accumulator-based line searches with simple and efficient peak extraction.
2. Graph-based clustering of projection peaks (via a Sphere-of-Influence graph [11]) that aggregates peaks into beam/column cross-section candidates, combined with outlier pruning and shape-based filtering to suppress clutter-induced responses.
3. Local geometric filtering in 2D using the neighborhood covariance to extract the corners of wall-encased structural elements.
4. A resulting set of simulation-oriented structural primitives: endpoints, and cross-section parameters (height and width), designed for straightforward export to downstream structural analysis and finite-element workflows.

2 Related Work

Scan-to-BIM and as-built modelling Scan-to-BIM research focuses on reconstructing semantically rich building models from point clouds, typically targeting components such as walls, floors, ceilings, or openings. These pipelines often prioritize completeness and semantic labeling over producing a structurally minimal model suitable for analysis [13, 15, 9]. In industrial buildings, where scans include extensive clutter and occlusions, BIM-oriented approaches frequently require significant preprocessing, manual intervention, or strong priors to separate load-bearing elements from non-structural geometry.

Scan-to-Finite Element Method and point-cloud-to-analysis pipelines Scan-to-FEM pipelines aim to derive geometry suitable for finite element simulation from scan data [14, 8, 12]. A common pattern is to reconstruct dense meshes or volumetric representations and then generate FE meshes for the scanned geometry. The literature also includes slicing- and voxelization-based approaches that work well for relatively clean scenes e.g., heritage structures [10, 1] or tunnels [2] where modelling most visible geometry is the intended result.

Structural element extraction by segmentation and primitive fitting A large class of methods treats structural element extraction as (i) segmentation of points into candidate components (manual or automatic), followed by (ii) primitive fitting (cuboids, cylinders [3], lines) and connectivity inference [6]. In practice, many pipelines become brittle in cluttered scans: segmentation is sensitive to density variation and occlusions, and primitive fitting can be misled by wall fragments, façade elements, and beam-wall intersections. Importantly, several approaches achieve good results only when the structural elements are pre-segmented (often manually) or when scans are restricted to the structural system itself.

Targeted skeleton extraction from full building scans Scan2Beams [7] is the closest method to the present work. It targets the same end goal: automatic extraction of axis-aligned beams and columns from full industrial building scans and export to a structural analysis representation, by discretizing the scene, accumulating projections on axis-aligned planes, detecting strong line carriers, clustering them into elements, and inferring joints by intersections. While effective as a proof of concept, Scan2Beams depends on several user-defined thresholds and a comparatively heavy detection stage (accumulator-based line detection), motivating the present paper's contribution toward faster, histogram-driven detection and streamlined clustering and filtering.

Existing Scan-to-BIM and Scan-to-FEM pipelines either (i) attempt full geometric reconstruction, which is unnecessarily expensive and brittle in cluttered industrial halls, or (ii) rely on strong assumptions such as pre-segmentation or clean scans. Scan2Beams [7] showed that targeted skeleton extraction is feasible directly from hall scans, but its detection stage remains computationally heavy and tuning-sensitive. We close this gap with a projection-driven detector that is substantially faster, and whose key threshold is chosen on an explicit histogram representation, making parameter selection visually interpretable while retaining robustness in in-the-wild scans.

3 Method

We are given a 3D point cloud $P = \{p_i \in \mathbb{R}^3\}$ representing a full building scan that contains both structural and non-structural geometry (e.g., walls, equipment, noise). Our goal is to extract a set of *structural elements* E consisting of beams and columns and to represent each element in a simulation-oriented form (endpoints and cross-section parameters) suitable for downstream structural analysis workflows.

We assume a layout in which the dominant structural system is *axis-aligned*. In practice, this is satisfied in most cases by an additional optional alignment step that estimates a global frame and rotates the point cloud accordingly. After this alignment step, candidate beams and columns are expected to be parallel to one of the principal axes $\{x, y, z\}$.

3.1 Overview

Our method is projection-driven and relies on the observation that axis-aligned structural elements create strong density peaks under orthogonal projection - Figure 2. For each principal axis $a \in \{x, y, z\}$ we:

1. build a 2D projection histogram on the orthogonal plane Π_a and extract the peaks,
2. cluster peaks into possible structure candidates using a proximity graph (Sphere-of-Influence) and reject outliers,
3. apply local geometric filtering to extract corners from wall-like and elongated non-structural elements,
4. lift each cluster back to 3D to fit a parametric beam/column primitive and export its parameters.

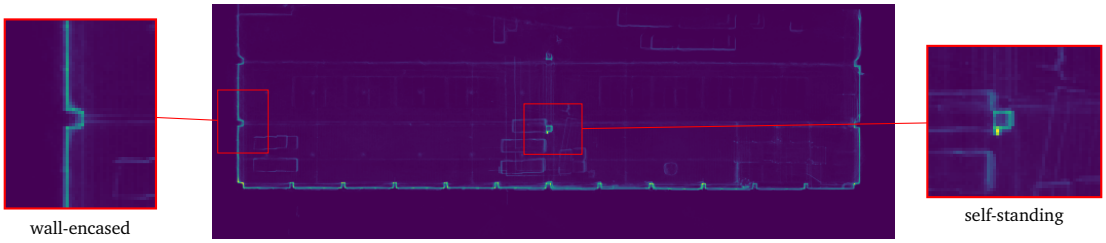

Figure 2: We project an example scene on the XY axes, and showcase examples of structural features highlighted in the histogram as peaks; on the left, structural elements that are part of the wall can be seen, motivating our corner extraction, while on the right, self-standing elements, such as support columns, show up as isotropic structures, motivating our aspect ratio constraints.

3.2 Projection histograms and peak extraction

For each axis $a \in \{x, y, z\}$, we define the orthogonal projection plane Π_a:

$$\Pi_x = yz, \qquad \Pi_y = xz, \qquad \Pi_z = xy,$$

and denote the orthogonal projection of point p by $\text{proj}_{\Pi_a}(p)$.

We discretize Π_a into a regular grid with cell size h and accumulate a 2D histogram

$$H_a(u,v) \;=\; \#\Big\{p \in P \;\Big|\; \text{proj}_{\Pi_a}(p) \in \text{cell}(u,v)\Big\}. \tag{1}$$

Intuitively, high-count bins correspond to locations where many 3D points share the same two coordinates and vary primarily along axis a, which is characteristic of axis-aligned structural elements.

We extract a set of peak locations

$$S_a = \Big\{(u,v) \;:\; H_a(u,v) \geq T \cdot max(H_a)\Big\},$$

where T is a user-defined threshold, between 0 and 1, defining the percentage of the maximum bin count that represents the peak thresholding. Each peak $s \in S_a$ defines a part of an *axis-aligned linear element* in 3D:

$$\ell(s,a) = \Big\{q \in \mathbb{R}^3 \;\Big|\; \text{proj}_{\Pi_a}(q) \in s\Big\}, \tag{2}$$

i.e., a locus of points that share the planar coordinates specified by cell s and are unconstrained along axis a.

3.3 Peak clustering into cross-section elements

A single beam or column typically induces multiple nearby peaks in Π_a, from the various faces and edges that appear in the scan. We therefore cluster peaks S_a, considering each bin's coordinates as vertices, to extract the contour of each element. We build a Sphere-of-Influence (SIG) graph [11] $SIG_a = (V_a, E_a)$ where $V_a = S_a$. Each vertex $s_i \in V_a$ is assigned an influence radius r_i equal to the distance to its nearest neighbor in V_a. Two peaks are connected if their influence regions overlap:

$$(s_i, s_j) \in E_a \quad \Longleftrightarrow \quad \|s_i - s_j\|_2 \leq (r_i + r_j).$$

We chose SIG for clustering because the input density is inherently captured in this graph, requiring no additional parameters, as additionally demonstrated in recent reconstruction works [4, 5]. Connected components of SIG_a yield peak clusters $\{C_a^k\}$. We refine these clusters, based on observations exemplified in Figure 2, using:

- **Outlier pruning:** remove vertices connected only through isolated long edges (i.e., edges much larger than the average edge length in SIG; in our experiments, removing edges larger than $3 \times avg$ yields good results).
- **Shape filtering:** compute the bounding box of each cluster and reject clusters with extreme aspect ratio, which are typical of wall-like or elongated structures. For example, for cluster $\{C_a^k\}$, using the cluster bounding box side lengths (w_k, h_k), reject if $\max(w_k, h_k)/\min(w_k, h_k) > \rho$, with $\rho = 10$ in our experiments. We chose a relatively high aspect ratio because some of the detected clusters contain a structural element surrounded by walls, and we do not want to remove such clusters too early.
- **Corner extraction:** remaining clusters are either containing 3 to 4 sides of a structural element, thus forming a cluster with isotropic contour (similar in shape to a square), or are non-isotropic, containing a corner structure and additional wall elements. We compute the covariance of each point that is part of the non-isotropic clusters, using its 2-ring in SIG. We use the ratio between the small and the large eigenvalues, and keep the largest 15% ratios as the corner points. We remove the rest, hence, removing points where the neighborhood does not exhibit a large variation on both principal axes. We only keep points that are part of corners, removing the additional wall pieces.

The remaining clusters localize candidate beam and column cross-sections on Π_a.

Scene	# Points	Histogram [ms]	SIG [ms]	SIG Filtering [ms]	Corner Filtering [ms]	Total [ms]
Scene 1	5,176,639	546.2	256.4	3.0	0.0	805.6
Scene 2	11,410,836	1616.3	404.1	5.0	7.0	2032.4
Scene 3	22,111,128	2360.7	533.5	2.0	9.0	2905.2
Scene 4	11,410,836	1377.6	317.6	3.4	4.0	1702.6
Scene 5	75,625,894	11827.6	964.0	3.0	0.0	12794.7
Scene 6	54,077,044	5526.7	666.5	1.0	6.0	6200.2
Scene 7	36,500,145	4122.1	472.1	2.0	1.0	4597.2
Scene 8	24,634,975	3089.3	1357.8	25.1	51.5	4523.7

Table 1: Timings of various pipeline parts in milliseconds. The corner filtering shows up as zero in some cases because this step does not get triggered unless there are non-square clusters left to process. We also observe that the histogram processing takes most of the time, which is to be expected, since this is the only step that deals with the full 3D dataset.

Method	1	2	3	4	5	6	7	8
Scan2Beams	39.06	86.53	476.37	129.44	1549.80	585.68	812.82	474.50
Ours	0.81	2.03	2.90	1.70	12.79	6.20	4.60	4.52
Speedup	≈ 48	≈ 43	≈ 164	≈ 76	≈121	≈ 94	≈177	≈ 105

Table 2: Runtime comparison (seconds) between our proposed method and Scan2Beams across all of our datasets. The Scan2Beams runtimes are not directly correlated with the number of points, and rather with the collection of parameters that need to be tuned, since those parameters affect the size of the data structure used internally. The Scan2Beams parameters are chosen to yield the best possible visual results.

3.4 Primitive estimation and output representation

Each cluster C_a^k corresponds to an element aligned with axis a. We estimate:

- **Endpoints:** we find all points that are projected into the cells of C_a^k and around $h/2$ padding around the contour, to mitigate any loss of information due to discretization. We find the minimal and maximal values along axis a to define the endpoints of the current structural element.
- **Cross-section parameters:** Use the projected points of this element in the orthogonal plane Π_a and fit a robust bounding rectangle, yielding width and height parameters.

The final output is a set of structural primitives

$$E = \{(e_0, e_1, \text{cross-section})\},$$

where (e_0, e_1) are endpoints, and `cross-section` stores the estimated profile parameters. This representation is designed for later usage in downstream structural analysis and finite element workflows (i.e., as node and line-element definitions with associated section properties).

4 Results

We evaluate our method on a collection of 8 in-the-wild point clouds of industrial building interiors captured through photogrammetry. The scans contain substantial non-structural geometry (e.g., walls, machinery, pipes) and exhibit typical artifacts such as occlusions, varying point density, and missing faces. Our scenes contain between $5M$ *and* $75M$ points. The absence of ground truth placements of structural elements prevents us from reporting exact precision/recall results for our datasets. Instead, we emphasize runtime, qualitative results, and focus on our application as a fundamental aid in the process of manual segmentation of such scenes.

Implementation details. All experiments were implemented in Python and run on a device with Intel i9-14900HX and NVIDIA 4090RTX. We report runtimes for the full pipeline and for the main processing stages in Table 1. We use a histogram cell size $h = 0.1$, peak threshold $T = 0.45 - 0.65$, depending on the number of structural elements expected in a given scan.

Timings. We compare against Scan2Beams [7], as the prior state-of-the-art in our setting, using their original implementation and parameterization, where possible. For fairness, both methods are applied to the same pre-aligned point clouds and run until the column/beam detection is performed, as the exporting is not time-consuming and can be adapted to various different formats. We report the results in Table 2, where we can observe a speedup of between 43× and 177× over the previous pipeline. We argue that, even if our proposed pipeline still requires 2 parameters to be tuned for good results, the quick results allow for much faster experiments compared to Scan2Beams. Additionally, both parameters can be easily related to the scene (size, density, and number of structural elements), while Scan2Beams requires a collection of absolute parameters that require multiple experiments and cannot easily be connected to the input.

(a) Example of broken assumptions.

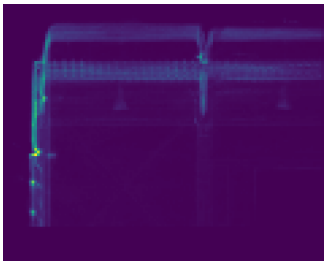

(b) Histogram on Π_y projection.

Figure 5: Scene 7 reconstruction, where our axis-aligned assumptions fail partially on one axis projection, due to the roof being formed of two parallel sections.

A second limitation is that cross-section estimation is currently simplified rather than being a dedicated, robust reconstruction step. A natural next step is to add a cross-section fitting stage (e.g., parametric profile fitting on filtered inliers in the orthogonal plane) after candidate extraction, improving geometric accuracy and exported simulation parameters.

Future work further includes relaxing the strict axis-alignment assumption (slanted members and local deviations), reducing parameter sensitivity via adaptive thresholding, and adding automatic joint classification to support direct import into structural engineering toolchains.

5 Conclusion

We presented a fast, projection-driven pipeline for extracting axis-aligned beams and columns directly from full building point clouds. The method leverages orthogonal projection histograms to obtain strong structural elements efficiently, clusters peak responses into location hypotheses using a graph-based grouping strategy, and refines candidates via local covariance descriptors to suppress wall-like and clutter-induced structures. The resulting elements are produced in a simulation-oriented representation (axis, endpoints, and associated parameters), enabling streamlined integration with structural analysis workflows. In practical building-scale scans, the approach substantially reduces the time-to-model compared to previous works while maintaining robustness to clutter and partial visibility.

References

[1] V. S. Alfio, D. Costantino, M. Pepe, and A. Restuccia Garofalo. A Geomatics Approach in Scan to FEM Process Applied to Cultural Heritage Structure: The Case Study of the "Colossus of Barletta". *Remote Sensing*, 14(3), 2022.

[2] L. Cui, L. Zhou, Q. Xie, J. Liu, B. Han, T. Zhang, and H. Luo. Direct generation of finite element mesh using 3D laser point cloud. *Structures*, 47:1579–1594, 2023.

[3] Y.-J. Liu, J.-B. Zhang, J.-C. Hou, J.-C. Ren, and W.-Q. Tang. Cylinder detection in large-scale point cloud of pipeline plant. *IEEE transactions on visualization and computer graphics*, 19(10):1700–1707, 2013.

[4] D. Marin, S. Ohrhallinger, and M. Wimmer. SIGDT: 2D Curve Reconstruction. *CGF*, 41(7):25–36, 2022.

[5] D. Marin, S. Ohrhallinger, and M. Wimmer. Parameter-Free Connectivity for Point Clouds. In *VISIGRAPP (1): GRAPP, HUCAPP, IVAPP*, pages 92–102, 2024.

[6] F. Noichl, A. Borrmann, and Y. Pan. Automated Steel Structure Model Reconstruction through Point Cloud Instance Segmentation and Parametric Shape Fitting. *Journal of Information Technology in Construction*, 30:1099–1122, 07 2025.

[7] J. Reisinger, D. Marin, P. Rufinatscha, and P. Kan. Scan2Beams: Moving Towards Automated Modelling and Analysis of Structural Industrial Building Stock. In *Proceedings of the 2025 European Conference on Computing in Construction*, volume 6 of *Computing in Construction*, Porto, Portugal, July 2025. European Council on Computing in Construction.

[8] B. Riveiro, G. Cubreiro, B. Conde, M. Cabaleiro, R. Lindenbergh, M. Soilán, and J. Caamaño. Automated Calibration of FEM Models using LIDAR Point Clouds. *The International Archives of the Photogrammetry, Remote Sensing and Spatial Information Sciences*, 42:969–974, 2018.

[9] R. Rolin, E. Antaluca, J.-L. Batoz, F. Lamarque, and M. Lejeune. From Point Cloud Data to Structural Analysis Through a Geometrical hBIM-Oriented Model. *J. Comput. Cult. Herit.*, 12(2), May 2019.

[10] Z. Selman, J. Musto, and L. Kobbelt. Scan2FEM: from Point Clouds to Structured 3D Models Suitable for Simulation. In *GCH*, pages 1–10, 2022.

[11] G. T. Toussaint. A graph-theoretical primal sketch. In *Machine Intelligence and Pattern Recognition*, volume 6, pages 229–260. Elsevier, 1988.

[12] W. Xu and I. Neumann. Finite Element Analysis based on A Parametric Model by Approximating Point Clouds. *Remote Sensing*, 12(3), 2020.

[13] L. Yang, J. C. Cheng, and Q. Wang. Semi-automated generation of parametric BIM for steel structures based on terrestrial laser scanning data. *Automation in Construction*, 112:103037, 2020.

[14] K. Yu, C. Zhang, M. Shooshtarian, W. Zhao, and J. Shu. Automated finite element modeling and analysis of cracked reinforced concrete beams from three dimensional point cloud. *Structural Concrete*, 22(6):3213–3227, 2021.

[15] S. Zbirovský and V. Nežerka. Open-source automatic pipeline for efficient conversion of large-scale point clouds to IFC format. *Automation in Construction*, 177:106303, 2025.

Posters

Image Vectorization with Generalized Coons Patches

Yan Jing[1], Kai Hormann[2], Chongyang Deng[1]

1 Faculty of Mathematics, Hangzhou Dianzi University, China
2 Faculty of Informatics, Università della Svizzera italiana, Switzerland

C⁰ Generalized Coons Patches

C⁰ Generalized Coons patches extend transfinite interpolation with classical Coons patches to arbitrary polygons and non-manifold topologies.

Mathematical Formulation

Let ϕ be the parameter domain with n vertices $\{v_k\}_{k=1}^{n}$, m internal points $\{v_k\}_{k=n+1}^{n+m}$ and edge set E.

$$S_{GC}(x) = \sum_{e_{i,j}\in E} (\lambda_i + \lambda_j)\cdot C_{i,j}\left(\frac{\lambda_i}{\lambda_i+\lambda_j}\right) - \sum_{k=1}^{n+m}(d_k - 1)\lambda_k p_k$$

λ_k: generalized barycentric coordinates of x associated with vertex v_k
$C_{i,j}(t)$: boundary curve associated with edge $e_{i,j}$, where $C_{i,j}(0) = p_i$, $C_{i,j}(1) = p_j$
p_k: corner point or interior control point
d_k: degree of v_k (2 for the boundary vertex, 0 for the interior control point)

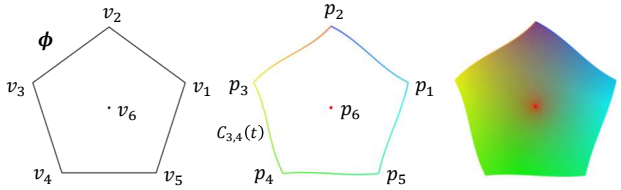

parameter domain + internal point | boundary curves | GC patch with interior point

Image Vectorization with GC Patches

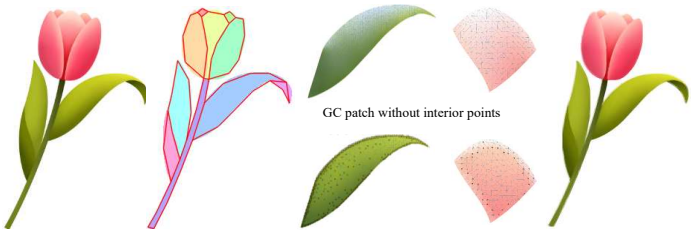

original image | segmented patch layout | GC patch with interior points | vectorization result

Each segmented region is treated as a GC patch. To reduce boundary-only reconstruction errors, a new interior control point is iteratively inserted at the parameter domain position of the pixel with largest error, until the global error falls below a threshold. Its color is then optimized by

$$\min_{P} \sum_{i\in\Omega} \|\hat{y}_i(P) - y_i\|_2^2 + w\sum_{m=1}^{M}\|P_m - y_m^*\|_2^2$$

Here, $P = [P_1, \ldots, P_M]$ denote the unknown RGB colors of all inserted interior control points to be solved, Ω is the set of fitting pixels, $\mathbf{y}_i$ and $\hat{\mathbf{y}}_i(P)$ are the ground-truth and reconstructed RGB values, and $\mathbf{y}_m^*$ is the ground-truth RGB value at the selected pixel.

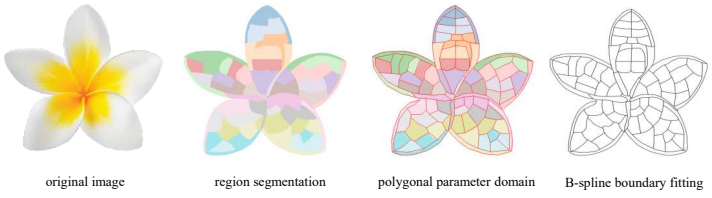

original image | region segmentation | polygonal parameter domain | B-spline boundary fitting

boundary color sampling | GC patch without interior points | adaptive insertion of interior points | vectorization result

Advantages

1. Arbitrary polygonal domains and fewer patches

The method supports arbitrary simple polygons as parametric domains, making it more suitable for complex image regions. It avoids the fold-over issues of traditional Coons patches, reduces the difficulty of parametric domain construction, and usually requires fewer segmented patches.

2. Adaptive interior control points for higher accuracy

Interior control points can be inserted adaptively in regions with large error. This makes the method easy to refine, while providing stronger expressive power and higher reconstruction accuracy.

RESULTS

Zoom-in Comparison

original image | vectorization result | zoom-in: original vs. vectorized

Reconstruction Results

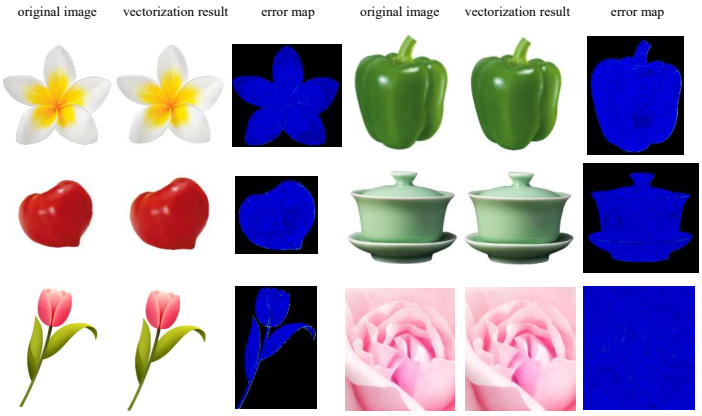

Editable Deformation

vectorization result | deformed vectorized result

REFERENCES

[1] Gerben Jan Hettinga, Jose Echevarria, and Jiri Kosinka. Efficient image vectorisation using mesh colours. Smart Tools and Apps for Graphics - Eurographics Italian Chapter Conference, 2021.

[2] Kaimin He, Jos B. T. M. Roerdink, and Jiri Kosinka. Image vectorization using a sparse patch layout. Graphical Models, 135:101229, 2024.

[3] Kaikai Qin, Yunhao Zhou, Chenhao Ying, Yajuan Li, and Chongyang Deng. C^0 generalized Coons patches for high-order cage-based deformation. ACM Transactions on Graphics, 43(6), 2024.

Speaker Index

Abid, Fatima-Ezzahrae (c) 24
Amri, Noura (c) 26
Antony, Joms (s) 39
Arhandou, Amine (c) 18
Bakadir, Salma (c) 13
Benroummane, Abderrazzak (c) 23
Bensad, Alaa Eddine (s) 31
Bonouali, Oumaima (c) 12
Boucetta, Mohammed (k) 6
Bradaai, Oumaima (c) 27
Celio, Marta (c) 16
El kacimi, Abdellah (k) 4
Favilli, Andrea (c) 9
Garau, Luca (c) 20
Jing, Yan (p) 53
Kzaz, Mustapha (c) 15
Lafdili, Hajar (c) 21
Lebzioui, Hicham (c) 25
Marin, Diana (s) 45
Naimi, Manal (c) 17
Ngadi, Soumia (c) 14
Polthier, Konrad (k) 5
Pottmann, Helmut (k) 3
Prautsch, Hartmut (c) 19
Salouani, Ranya (c) 22
Singh Bedi, Navdeep (c) 10
Zaidane, Fadwa (c) 11

c ..... contributed talk
k ..... keynote talk
p ..... poster
s ..... short paper